

Chapter Four

RESULTS AND DISCUSSION

4.1 Introduction

As reviewed in Chapter 2, it was shown that various types of physicochemical separation methods such as distillation, ion exchange chromatography and liquid/liquid extraction have been used to separate the ^{68}Ga radionuclide from the ^{68}Ge radionuclide. It was shown by De Blois et al., (2011); Breeman et al. (2004) and Velikyan et al., (2004), that several types of $^{68}\text{Ge}/^{68}\text{Ga}$ materials for the absorption of ^{68}Ga with different inorganic absorption materials for the absorption of ^{68}Ga existed.



Commercially available TiO_2 materials proposed since the 1970's as very promising ion exchangers for ^{68}Ge and ^{68}Ga radionuclides for medical use (Kopecky et al., 1973; Mirzadeh and Lambrecht, 1995). It was also shown by Kozlova et al., (1970) that ion exchange chromatography using TiO_2 in low hydrochloric acid mixtures also gave very promising results for the separation of ^{68}Ge from ^{68}Ga . The adsorption capacity for Ge^{+4} is approximately 120 mg Ge per gram sorbent in 0.1 M HCl solutions. Furthermore, the distribution coefficient (K_d) is greater than 10 000 ml/g for carrier-free $^{68}\text{Ge}^{+4}$ ions and 2 ml/g for $^{68}\text{Ga}^{+3}$, when evaluated in 0.1 M HCl solution. Lastly, the decision to perform ^{68}Ga elutions with 0.1 M HCl seemed to be an advantage for further labelling studies with the ^{68}Ge radionuclide.

In the present study the investigations were limited to evaluating only the TiO_2 matrix as an absorption material. Experimental evidence also revealed that heating TiO_2 metal oxide to a temperature exceeding 400 °C, caused an irreversible change which was supported by observing yellowing of the TiO_2 . Brady (1971) writes that rutile is a high temperature stable

phase and anatase, on the other hand, is a lower temperature phase. Therefore, a decision was taken to heat anatase up to 400 °C whilst rutile was heated to temperatures of up to 850 °C, as set out in Table 4.6. After the milling and sieving of the appropriate TiO₂ samples from the various suppliers, the structural characterization of the TiO₂ metal oxide materials was carried out using various analytical techniques such as X-ray Diffraction (XRD), X-ray Fluorescence (XRF), and Scanning Electron Microscopy (SEM). TiO₂ was analyzed by X-ray diffraction (XRD) for phase identification and crystallite size estimation. The XRD patterns obtained for the TiO₂ metal oxide materials using the method given in section 3.4.1 are shown in Figure 4.1 to Figure 4.6.

4.2 XRD – Mineral phase Analysis

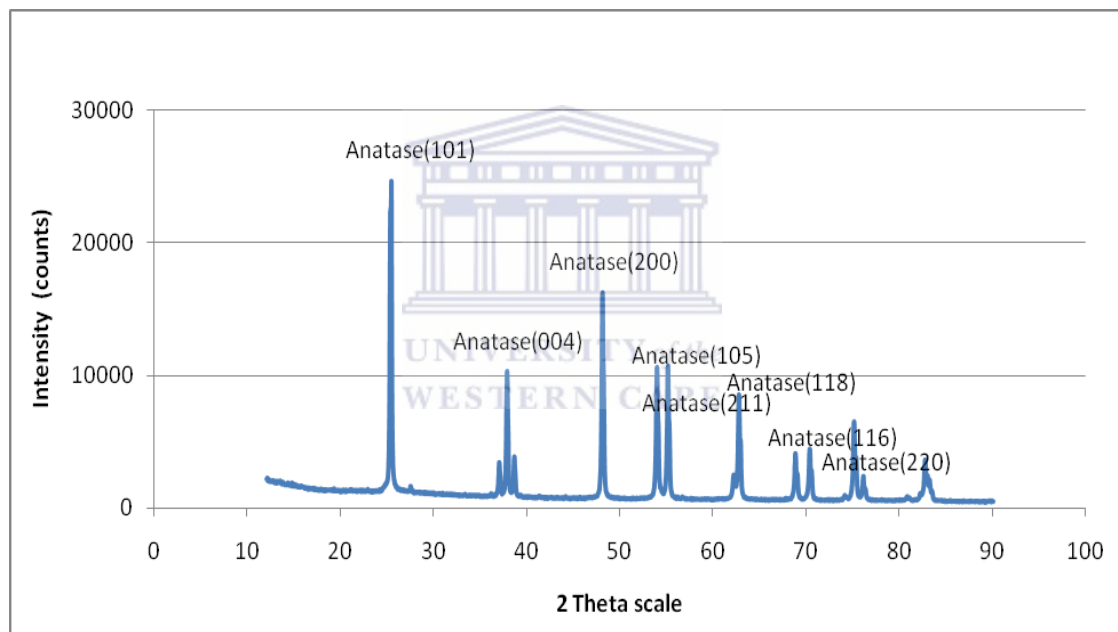


Figure 4.1: X-ray diffraction of the TiO₂A₁ from Sigma-Aldrich

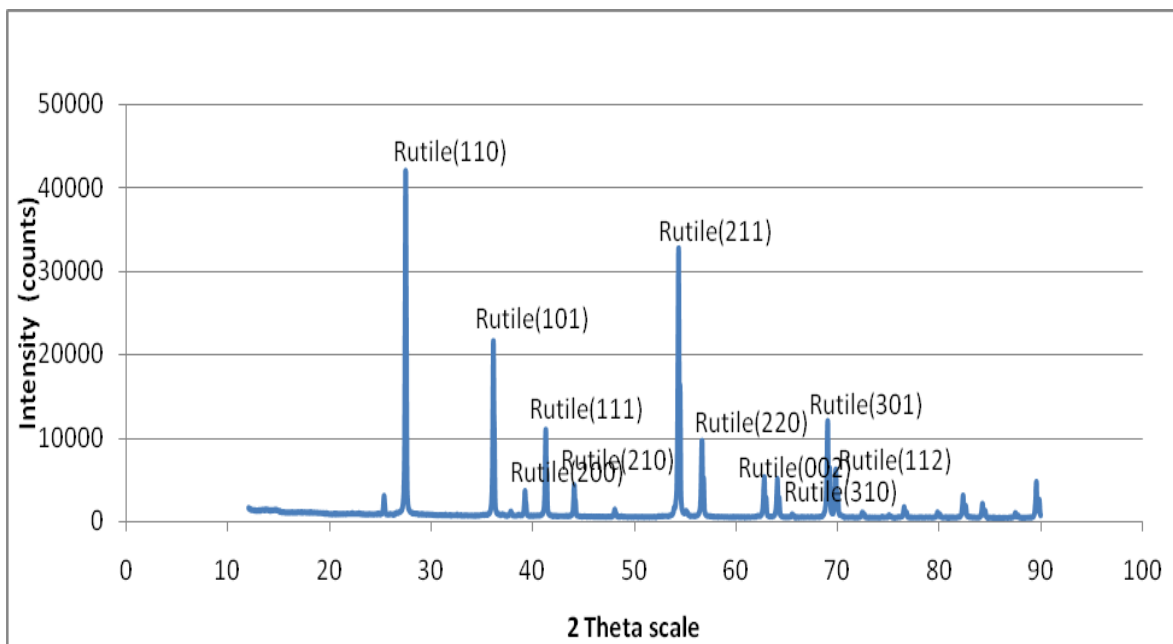


Figure 4.2: X-ray diffraction of the TiO₂A₂ from Sigma-Aldrich

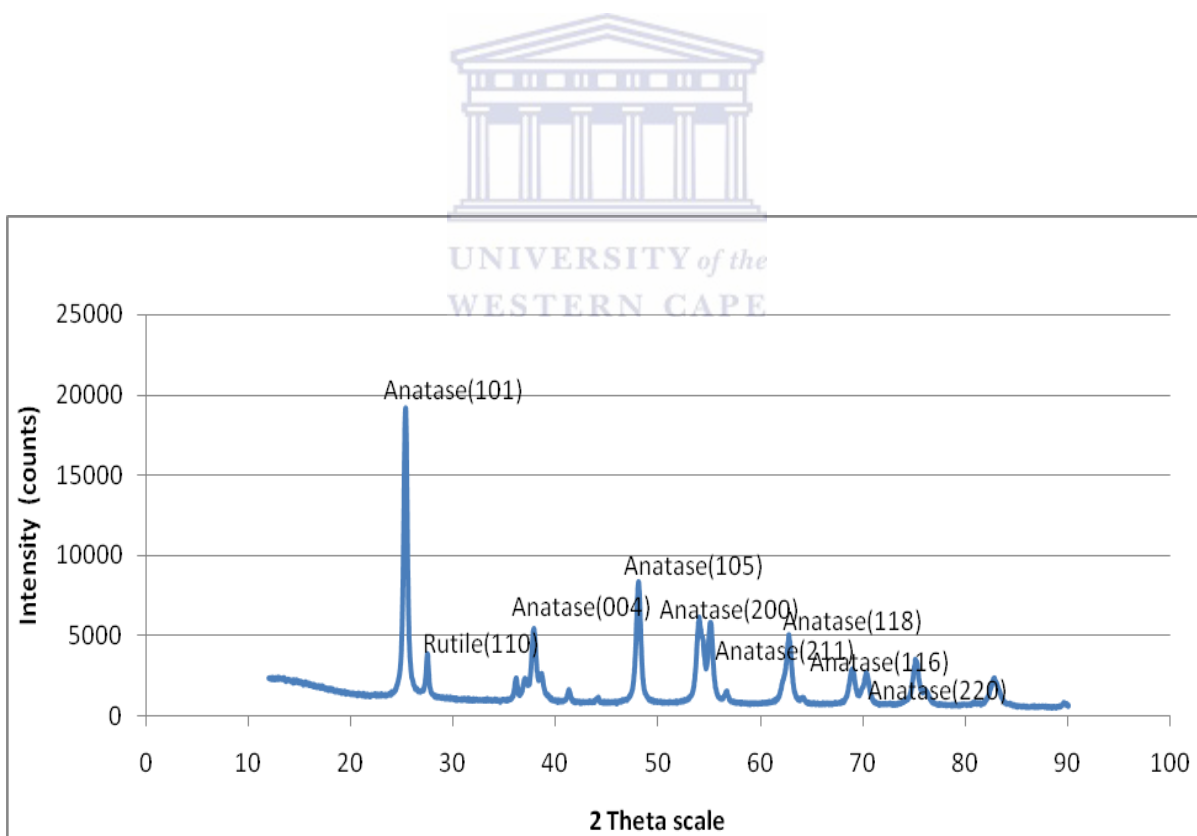


Figure 4.3: X-ray diffraction of the TiO₂A₃ from Evonik Industries; unheated

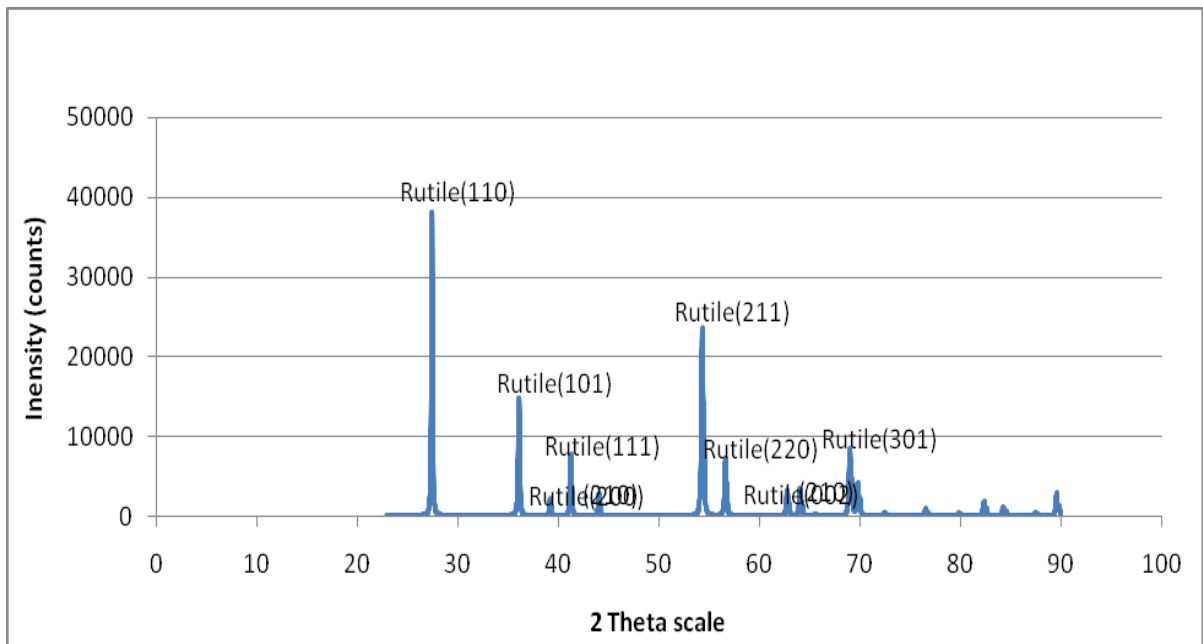


Figure 4.4: X-ray diffraction of the TiO_2A_3 from Evonik Industries; heated at 850°C for 3 hours

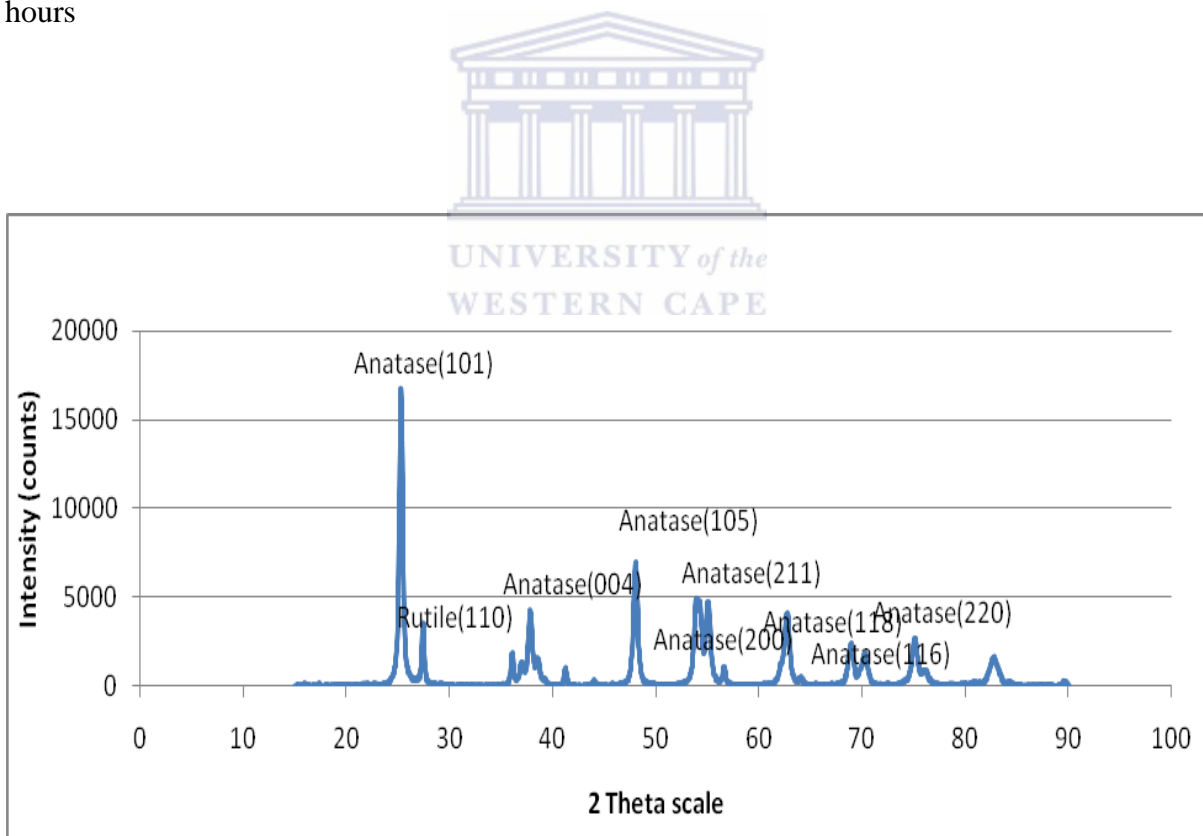


Figure 4.5: X-ray diffraction of the $90\text{-}212\ \mu\text{m}$ TiO_2A_4 from Evonik Industries; unheated

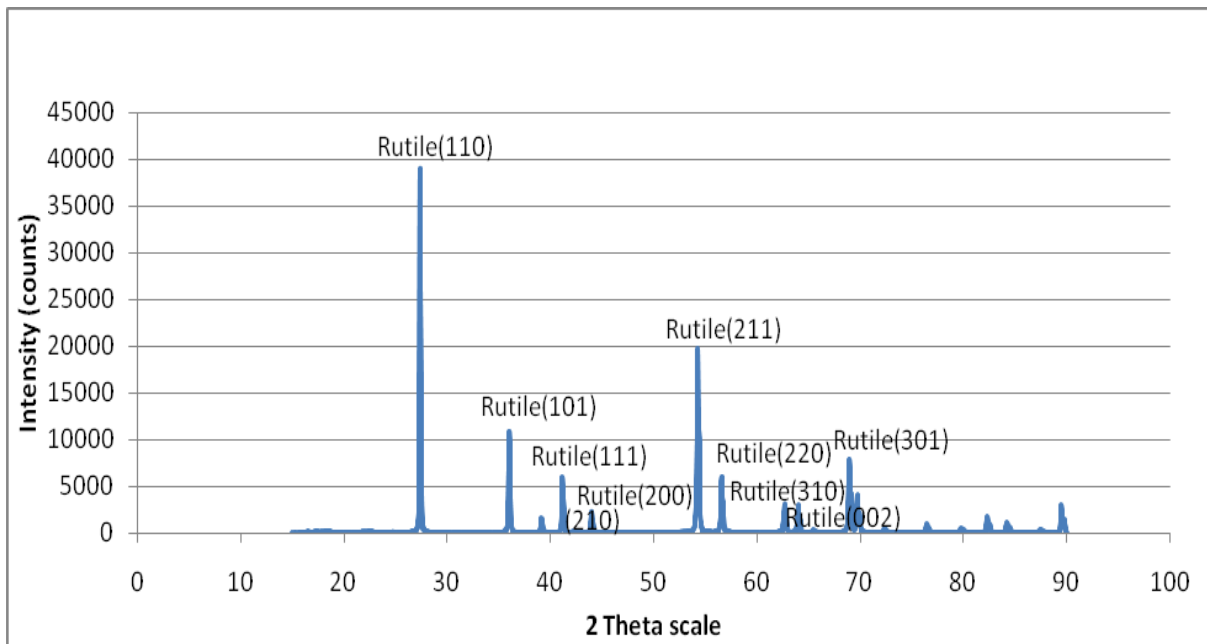


Figure 4.6: X-ray diffraction of the 90-212 μm TiO_2A_4 from Evonik Industries; heated at 850 $^\circ\text{C}$ for 3 hours

Figure 4.1 shows the X-ray diffraction patterns of the TiO_2A_1 (anatase) without temperature to prevent phase transformation from anatase to rutile. Analysis of the X-ray diffraction patterns of the TiO_2A_1 revealed the presence of one phase: anatase. Quantification was possible because the intensity of the diffraction pattern of a phase depends on its concentration. The intensity data showed that the material contained 100% of anatase and no rutile material was present. No peak broadening was observed due to large crystallite size effect when compared to diffraction patterns of the various commercial TiO_2 sources. By using Scherrer's formula (equation 2.4), the crystallite size of the TiO_2A_1 powder was found to be 12.16 nm.

Figure 4.2 shows the X-ray diffraction patterns of the TiO_2A_2 (rutile) without temperature to prevent phase transformation from anatase to rutile. As before, analysis of the X-ray diffraction patterns of the TiO_2A_2 revealed the presence of one phase: rutile. The intensity data showed that the material contained 100% of rutile and no anatase material was present. Again, no peak broadening was observed due to large crystallite size effect when compared to diffraction patterns of the various commercial TiO_2 sources. By using Scherrer's formula (equation 2.4), the crystallite size of the TiO_2A_2 powder was found to be 11.10 nm.

Figure 4.3 shows the X-ray diffraction patterns of the TiO_2A_3 (anatase) without temperature to prevent phase transformation from anatase to rutile. Analysis of the X-ray diffraction patterns of the TiO_2A_3 revealed the presence of two phases: anatase and rutile in different weight percentages. Once again, quantification was possible because the intensity of the diffraction pattern of a phase depended on its concentration. The intensity data showed that the material contained 95% of anatase and about 5% rutile material was present. Peak broadening was observed due to small crystallite size effect when compared to diffraction patterns of the various commercial TiO_2 sources. By using Scherrer's formula (equation 2.4), the crystallite size of the TiO_2A_3 powder was found to be 12.15 nm.

Figure 4.4 shows the X-ray diffraction patterns of the TiO_2A_3 (anatase) heat treated in the Carbolite furnace at 850 °C for 3 hours. This diffraction pattern changed to 100% rutile phase structured TiO_2 peaks at 850 °C. The TiO_2A_3 powder which has a 95% rutile phase structure and 5% anatase phase structure with an average particle size of 12.15 nm had undergone phase transformation from the anatase phase structure to the rutile phase structure during heating. Again, no peak broadening was observed due to large crystallite size effect when compared to diffraction patterns of the various commercial TiO_2 sources. By using Scherrer's formula (equation 2.4), the crystallite size of the heat treated TiO_2A_3 powder was found to be 24.43 nm.

Figure 4.5 shows the X-ray diffraction patterns of the TiO_2A_4 (anatase) without temperature to prevent phase transformation from anatase to rutile. Analysis of the X-ray diffraction patterns of the TiO_2A_4 revealed the presence of two phases: anatase and rutile in different weight percentages. Once again, quantification was possible because the intensity of the diffraction pattern of a phase depended on its concentration. The intensity data showed that the material contained 95% of anatase and about 5% rutile material was present. Peak broadening was observed due to small crystallite size effect when compared to diffraction patterns of the various commercial TiO_2 sources. By using Scherrer's formula (equation 2.4), the crystallite size of the TiO_2A_3 powder was found to be 11.05 nm.

Figure 4.6 shows the X-ray diffraction patterns of the TiO_2A_4 (anatase) heat treated in the Carbolite furnace at 850 °C for 3 hours. This diffraction pattern changed to 100% rutile

phase structured TiO₂ peaks at 850 °C. The TiO₂A₄ powder which has a 95% rutile phase structure and 5% anatase phase structure with an average particle size of 21.37 nm had undergone phase transformation from the anatase phase structure to the rutile phase structure during heating. Again, no peak broadening was observed due to large crystallite size effect when compared to diffraction patterns of the various commercial TiO₂ sources. By using Scherrer's formula (equation 2.4), the crystallite size of the heat treated TiO₂A₃ powder was found to be 21.37 nm.

Common to all the figures, the peaks located at $2\theta = 27.5, 36.1, 54.4$ corresponded to the (110), (101), (211) planes of the rutile phase (JCPDS 21-1276) and the peaks located at $2\theta = 25.4, 37.8, 48.0, 54.5$ corresponded to the (101), (004), (200), (105 and 211) planes of the anatase phase (JCPDS 21-1272), respectively. Furthermore, the intense diffraction lines like (110) and (101) indicated high crystallinity. Generally, anatase will transform into rutile at $\sim 600^\circ\text{C}$ (Depero et al., 1993). An investigation of intensities showed that when no heat was applied to the TiO₂ samples (Figure 4.1, 4.3 and 4.5), the diffraction peaks were broad indicating small crystallite size and the broadening decreased with temperature (Figure 4.2, 4.4 and 4.6). Also, when heat was applied, intensities were observed in the region of 40 000 counts, implying strong crystallization from the samples. In turn, when heat was not applied, intensities were observed in the region of 20 000 counts, implying lower crystallinity.

The position (2θ) and the full width at half height (FWHM) were used to identify the particle size of the TiO₂ metal oxide examined (Table 4.1). When particle size became smaller, the peaks became broad (Figure 4.3 and Figure 4.5) and the width larger. The broadening occurs due to micro strains of the crystal structure arising from defects like dislocation and twinning (Zhang et al., 2011). The anatase (101) and rutile (110) peaks were used to determine the grain size by Scherrer's formula. The results of the grain size analysis are shown in Table 4.1.

Table 4.1: XRD Data of the TiO₂ Materials

TiO ₂ Type	2θ	θ	Cos θ	Sin θ	FWHM (°)	FWHM (radians)	Size (nm)
TiO ₂ A ₁	25.4	12.7	0.9755	0.2198	0.70	0.0122	12.16
TiO ₂ A ₂	27.7	13.9	0.9707	0.2402	0.77	0.0134	11.10
TiO ₂ A ₃ u	25.1	12.6	0.9759	0.2174	0.70	0.0122	12.15
TiO ₂ A ₃ h	27.7	13.9	0.9707	0.2402	0.35	0.0134	24.43
TiO ₂ A ₄ u	25.4	12.7	0.9755	0.2198	0.77	0.0134	11.05
TiO ₂ A ₄ h	27.6	13.8	0.9711	0.2385	0.20	0.0126	21.37

It was concluded that the phase structure and the particle size could play an important role in the ⁶⁸Ge loading of the titanium dioxide based ⁶⁸Ge/⁶⁸Ga generator system. From the XRD data, it was evident that the crystallite size increased with temperature and that the diffraction peaks became more intense and their FWHM gradually became narrower suggesting an increase in particles size and increase in the amount of the relevant phase.

4.3 XRF- Elemental Analysis

For XRF analysis, a decision was taken to only investigate the chemical composition of the TiO₂A₃ Aeroxide and TiO₂A₄ Aerolyst metal oxide from Evonik due to the promising results obtained when the two materials were investigated for ⁶⁸Ge loading and ⁶⁸Ga desorption, as set out in section 3.4.2. The weight percent of the metal oxides using the XRF technique is given in Table 4.2.

Table 4.2: Chemical composition of TiO₂A₃ and TiO₂A₄ metal oxides by XRF (weight %) (n=3)

Sample	V ₂ O ₅	TiO ₂	K ₂ O	P ₂ O ₅	Al ₂ O ₃	MgO	Na ₂ O	LOI	Total
*CRM 61	0.45	93.38	0.06	0.05	1.18	0.17	0.10	0.31	98.17
TiO ₂ A ₃ u	0.27	95.09	0.06	0.01	0.00	0.10	0.65	3.05	99.44
TiO ₂ A ₃ u	0.28	95.34	0.06	0.01	0.00	0.10	0.67	3.05	99.53
TiO ₂ A ₃ u	0.27	95.28	0.06	0.01	0.00	0.10	0.66	3.05	99.45
TiO ₂ A ₃ h	0.27	98.91	0.00	0.01	0.00	0.05	0.00	0.21	99.63
TiO ₂ A ₃ h	0.27	99.20	0.00	0.01	0.00	0.06	0.00	0.21	99.75
TiO ₂ A ₃ h	0.28	99.18	0.00	0.01	0.00	0.07	0.00	0.21	99.76
TiO ₂ A ₄ u	0.28	97.38	0.00	0.01	0.00	0.07	0.03	1.27	99.04
TiO ₂ A ₄ u	0.28	97.41	0.00	0.01	0.00	0.07	0.05	1.27	99.09
TiO ₂ A ₄ u	0.27	97.56	0.00	0.00	0.00	0.07	0.03	1.27	99.21

*Certified Reference Material (External source: Scientific Services measurement facility)

Table 4.3: Statistical Analysis of the TiO₂A₃ and TiO₂A₄ XRF experimental data

Sample	A (%)	B (%)	C (%)	Average (%)	Standard Deviation (%)	Relative Standard Deviation (%)
TiO ₂ A ₃ u	99.44	99.53	99.45	99.4733	0.0493	0.050
TiO ₂ A ₃ h	99.63	99.75	99.76	99.7133	0.0723	0.070
TiO ₂ A ₄ u	99.04	99.09	99.21	99.1133	0.0874	0.090

The chemical composition of the TiO₂A₃ and TiO₂A₄ samples revealed the presence of the following elements: V₂O₅, TiO₂, CaO, K₂O, P₂O₅, Al₂O₃, MgO, and NaO. This procedure was performed in triplicate to ensure its reliability. Analysis results had good relative precision (repeatability) (see Table 4.3). Before TiO₂ sources were analyzed, the samples were dried to permit accurate weighing. As said before (Experimental section 3.4.2), the loss on ignition (LOI) was determined by first weighing approximately 1 g sample of TiO₂ followed by heating at 900 °C for 30 minutes, weighed again, then heated for another 60 minutes at the same temperature and weighed for a third time.

While it was desirable for the impurities of the TiO₂ sources to be less than 1%, extended drying was not carried out to avoid possible over-drying problems. These might result in hardness and probably phase change. The XRF results (Table 4.2) indicated that TiO₂A₃h was the purest of the three TiO₂ sources, as the impurities were less than 1%. The same cannot be said for the TiO₂A₃u and TiO₂A₄u sources as they had impurities that were more than 1%. The results in Table 4.2 revealed larger LOI values (3.27 for TiO₂A₃u and 1.27 for TiO₂A₄u), indicating high moisture content in the TiO₂ sources. It was noted that such large LOI values were the results of the more than 1% impurity levels obtained for the TiO₂A₃u and TiO₂A₄u sources. The moisture content can be solved by introducing other means of drying but again the loading of ⁶⁸Ge can be affected if complex means are adopted. A simple, short and less complicated drying mechanism was preferred, because no phase change could occur while the source is undergoing drying.

4.4 SEM- Surface Morphology Analysis

Next, Scanning Electron Microscopy (SEM) was carried out to analyse the effect of heat treatment on the surface morphology of the TiO₂A₃ and TiO₂A₄ samples. The experimental

procedure for the SEM technique is detailed in section 3.4.3. The generated SEM microgram images are shown in Figure 4.10.

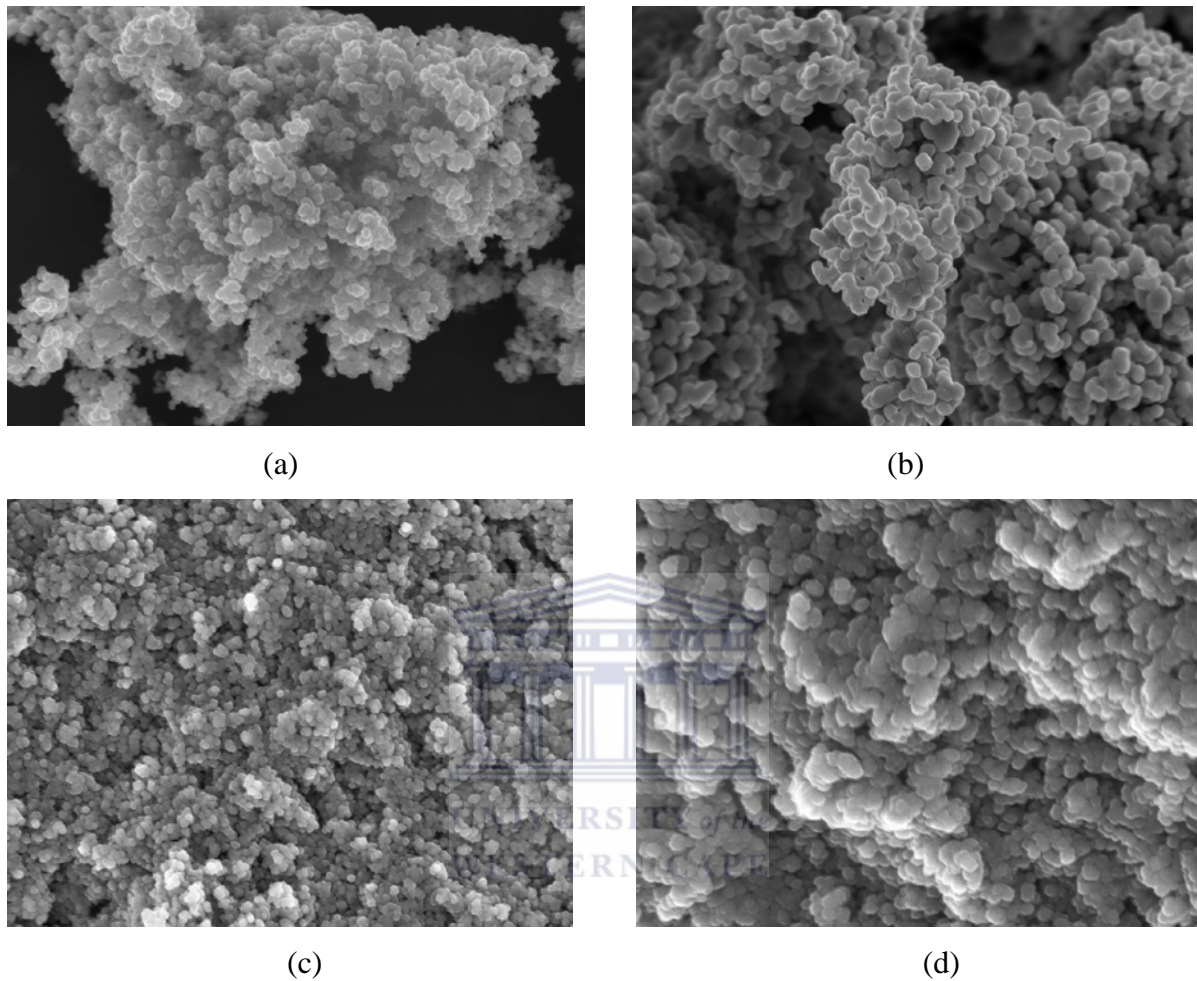


Figure 4.7: Scanning Electron Microscopy (SEM) micrographs of the carbon-coated TiO_2A_3 and TiO_2A_4 metal oxides; (a) TiO_2A_3 (unheated) (x200), (b) TiO_2A_3 (heated at 850 °C for 3 h)(x200), (c) TiO_2A_4 (90-212 μm , unheated)(x200), (d) TiO_2A_4 (90-212 μm , heated) (x100) (External source: University of the Western Cape measurement facility)

The observed micro-structural characteristics of the TiO_2A_3 and TiO_2A_4 samples revealed a fine grained structure suggestive of a crystalline matrix. In the first SEM image, Figure 4.7(a), the TiO_2A_3 untreated sample displayed an irregular shaped particulate morphology compared to the more spherical shaped particulate morphology exhibited by TiO_2A_3 in Figure 4.7(b). Moreover, the SEM image of 4.7(c) corresponding to the TiO_2A_4 unheated, demonstrates that the particle size of the material is smaller than that of the TiO_2A_3 , but both displayed crystallite particles on the surface which was in agreement with XRD detection.

Also, there is some particle agglomeration observed in all images. Statistical analysis of different SEM images showed that the average diameter of the agglomerated particles was in the range of 10 -30 nm.

4.5 TEM- Particle Analysis

In order to see the individual TiO_2 particles of the TiO_2A_3 and TiO_2A_4 samples, analysis of the TiO_2 powdered samples was done using the transmission electron microscopy (TEM) technique. The experimental procedure for TEM technique is detailed in section 3.4.4. Images of the TiO_2A_3 and TiO_2A_4 samples can be seen in Figure 4.8.

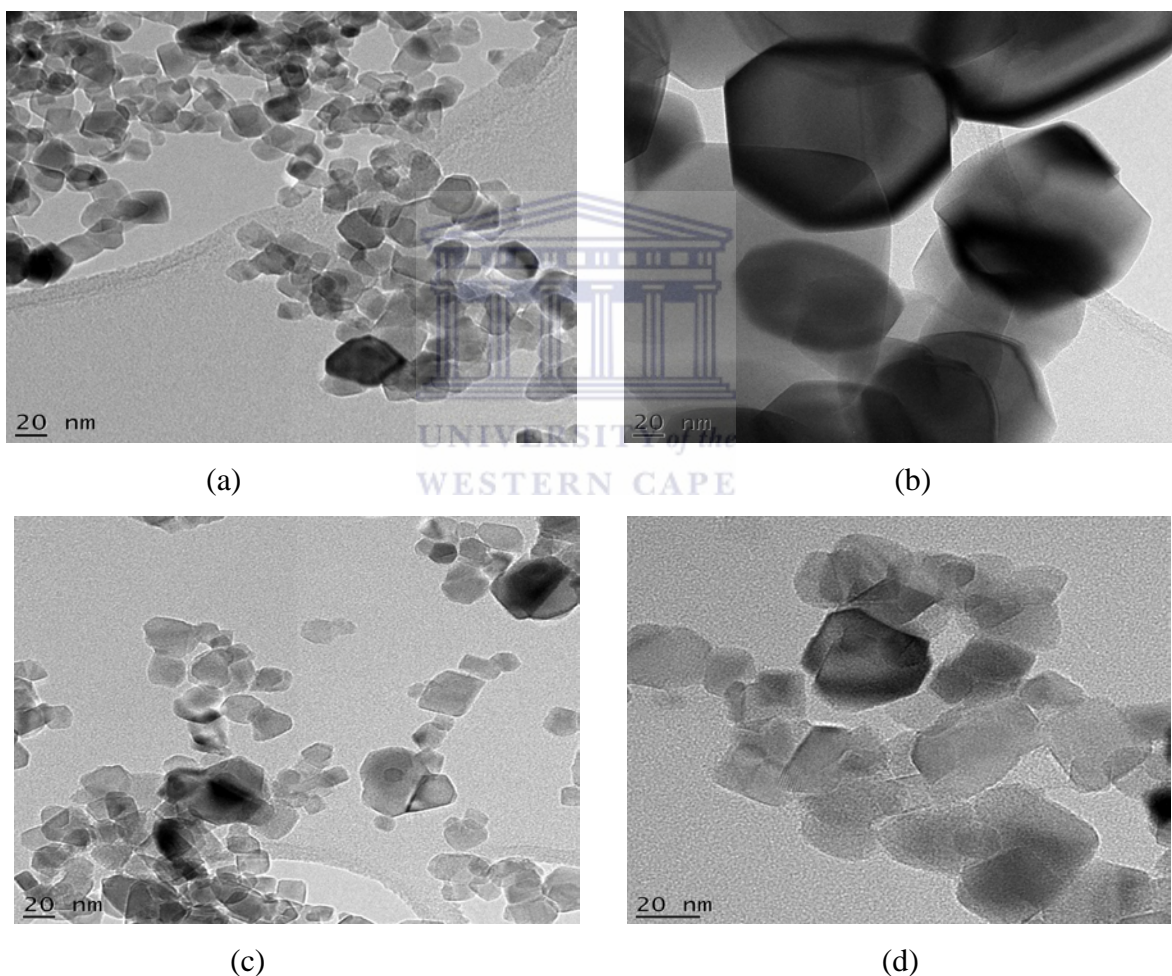


Figure 4.8: Transmission Electron Microscopy (TEM) micrographs of the carbon-coated TiO_2A_3 and TiO_2A_4 metal oxides; (a) TiO_2A_3 (unheated) (x200), (b) TiO_2A_3 (heated at 850 °C for 3 h) (x200), (c) TiO_2A_4 (90-212 μm , heated) (x200), (d) TiO_2A_4 (90-212 μm , heated) (x100) (External source: University of the Western Cape measurement facility)

Initial TEM examination of the samples using TEM showed that the particles were in hexagonal structure, which was not visible from the images observed using SEM. The images shown in Figures 4.8(a) and 4.8(b) revealed that the TiO_2A_3 samples were not only uniform but also well dispersed compared to that of sample TiO_2A_4 in Figures 4.8(c) and 4.8(d). It can be seen that there is an obvious growth in the particle size between Figures 4.8(a) and 4.8(b), due to heat-treatment of the sample. Consequently, the difference in the particle size can be attributed to the heat treatment and phase transformation. This phenomenon is in agreement with results reported by other investigators (Depero et. al., 1993; Goldstein, 2003; Egerton, 2005). Figures 4.8(c) and 4.8(d) presents the TiO_2A_4 without heat. Based on the TEM micrographs, the size of individual particles was measured using image-analyzing methods and found to be ~ 19 nm. In any event the driving force for morphological shape change to the rutile structure will be the overall reduction in surface energy. Theoretically, the presence of an amorphous film on the surface will clearly affect the surface energy, aid the movement of ionic species and hence speed the changes in morphology of the structure.

4.6 BET- Surface Area Analysis

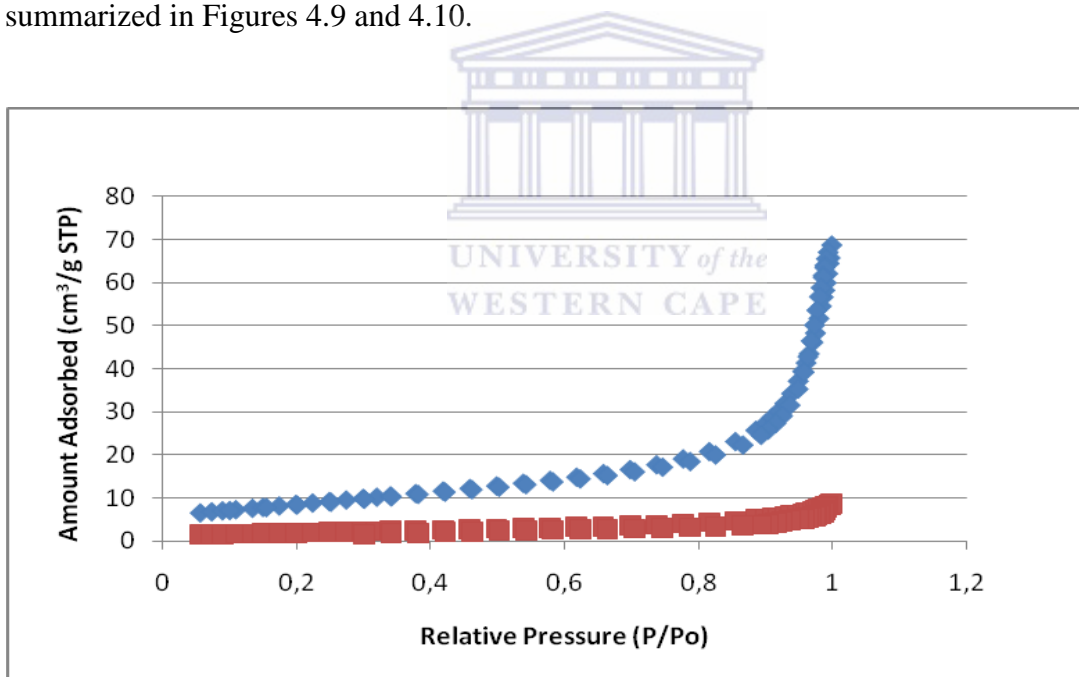
In order to explore the specific surface area of the TiO_2A_3 and TiO_2A_4 sources, BET analyses were determined by physical adsorption of a nitrogen gas on the surfaces of the solids (see Experiment 3.4.5). As a high ^{68}Ge uptake correlates with a high specific surface area of the TiO_2 source, the varying ^{68}Ge uptake were explained when the expression of the surface area was studied. Thereafter, from the volumetric adsorption measurements of each sample, respective isotherms were drawn to visualize key factors such as surface areas, pore sizes and pore volumes which may be responsible for providing useful information in developing a test model that loads ^{68}Ge successfully onto the TiO_2 sources. Table 4.4 shows the pore characteristics of the heated and unheated TiO_2 sources obtained by the nitrogen sorption measurements.

Table 4.4: Summary of BET Surface Areas of the TiO_2A_3 and TiO_2A_4 sources

Sorbent	Surface Area (m^2/g)	Mean Pore Size (nm)	Mean Pore Volume (cm^3/g)
$\text{TiO}_2\text{A}_3\text{u}$	31.2147	7.28553	0.101590
$\text{TiO}_2\text{A}_3\text{h}$	7.2003	13.01821	0.013115
$\text{TiO}_2\text{A}_4\text{u}$	45.5329	9.81666	0.111745
$\text{TiO}_2\text{A}_4\text{h}$	0.2574	12.96791	0.000834

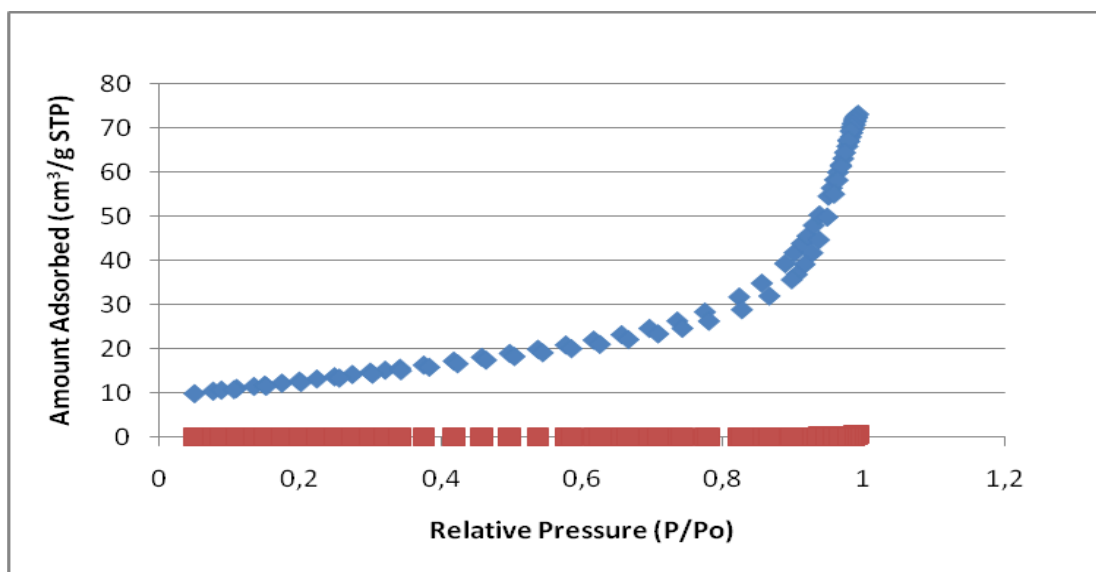
From the data, the immediate observation was that the unheated TiO_2A_3 sample ($\text{TiO}_2\text{A}_{3\text{u}}$) showed a higher surface area ($31.2147 \text{ m}^2/\text{g}$) and pore volume ($0.101590 \text{ cm}^3/\text{g}$) when compared to the heated sample ($7.2003 \text{ m}^2/\text{g}$ and $0.013115 \text{ cm}^3/\text{g}$, respectively). This trend was additionally supported by the TiO_2A_4 sample. The averages of the pore sizes and the averages of pore volumes are also presented in Table 4.4. However, the data show no clear distinction between the heated and unheated samples. Therefore, a much more detailed investigation will be to look at parameters such as the pore size distributions and the micro pore volumes. The two parameters will be discussed in this section.

Ideally the surface area should be increased so that it can allow adsorption of as much ^{68}Ge radionuclide as possible without complicated chemical manipulation. In order to load the ^{68}Ge effectively for ^{68}Ga generator investigation, the larger surface area is most desirable. The nitrogen adsorption-desorption isotherms of the TiO_2A_3 and TiO_2A_4 sources are summarized in Figures 4.9 and 4.10.



(a) ◆ TiO_2A_3 (unheated); (b) ■ TiO_2A_3 (heated)

Figure 4.9: Comparison of N_2 sorption isotherms at $-196 \text{ }^\circ\text{C}$ of (a) TiO_2A_3 (unheated) and (b) TiO_2A_3 (heated at $850 \text{ }^\circ\text{C}$) from Evonik Industries by BET analysis (External source: University of Cape Town measurement facility)



(a) \blacklozenge TiO_2A_4 (unheated); (b) \blacksquare TiO_2A_4 (heated)

Figure 4.10: Comparison of N_2 sorption isotherms at $-196\text{ }^\circ\text{C}$ of (a) $90\text{-}212\text{ }\mu\text{m}$ TiO_2A_4 (unheated) and (b) $90\text{-}212\text{ }\mu\text{m}$ TiO_2A_4 (heated at $850\text{ }^\circ\text{C}$) from Evonik Industries by BET analysis (External source: University of Cape Town measurement facility)

During the N_2 adsorption process of the heated and unheated TiO_2A_3 samples, the plots exhibited completely reversible isotherms, where the adsorption and desorption of the N_2 with slight hysteresis was observed. Detailed comparisons between the heated and unheated TiO_2A_3 samples showed a higher N_2 adsorption by the unheated sample (Figure 4.9), indicating the porous nature of the sample. On the other hand, the low N_2 adsorption exhibited by the heated N_2 adsorption showed the non-porous nature of the sample. The shape of the isotherms indicated that TiO_2A_3 is dominantly macroporous. The hysteresis was extremely narrow on both TiO_2A_3 samples and this indicated the presence of fine macropores. Another marked observation was the low adsorbed volume at $P/P_0 < 0.01$, an indication that TiO_2A_3 had negligible or non-existent micropores.

Figure 4.10 shows the N_2 adsorption/desorption isotherms of the TiO_2A_4 . During the process of N_2 adsorption on the unheated TiO_2A_4 , as before, adsorption of N_2 occurred at relatively high pressure when compared to the heated samples. There is a noticeable similarity in the shapes that the two unheated samples exhibit, indicating a consistent relation for the two TiO_2 sources. Comparing the two curves of the heated sample TiO_2A with that of the unheated

sample, it can be seen that the adsorption capacity for the heated TiO_2A_4 sample was extremely low, practically nil, as measured in this work. From the previous surface area discussion, it can be seen that the heated samples did not perform at all; and the curves obtained were broadly consistent with the XRD, SEM and TEM results. Again, the hysteresis was narrow but visible for the unheated TiO_2A_4 samples, indicating a significant presence of fine macropores.

On the other hand, the gas phase in pores with different diameters will condense at different pressures and thus provide quantitative information about the relative volume of different pore-sizes in the TiO_2 samples. The pore-size distribution (PSD) is obtained by application of a BJH (Barret, Joyner, and Halenda) technique (Raj and Viswanathan, 2009). Results of pore-size distribution from the four TiO_2 samples are presented in Figure 4.11 for comparison.

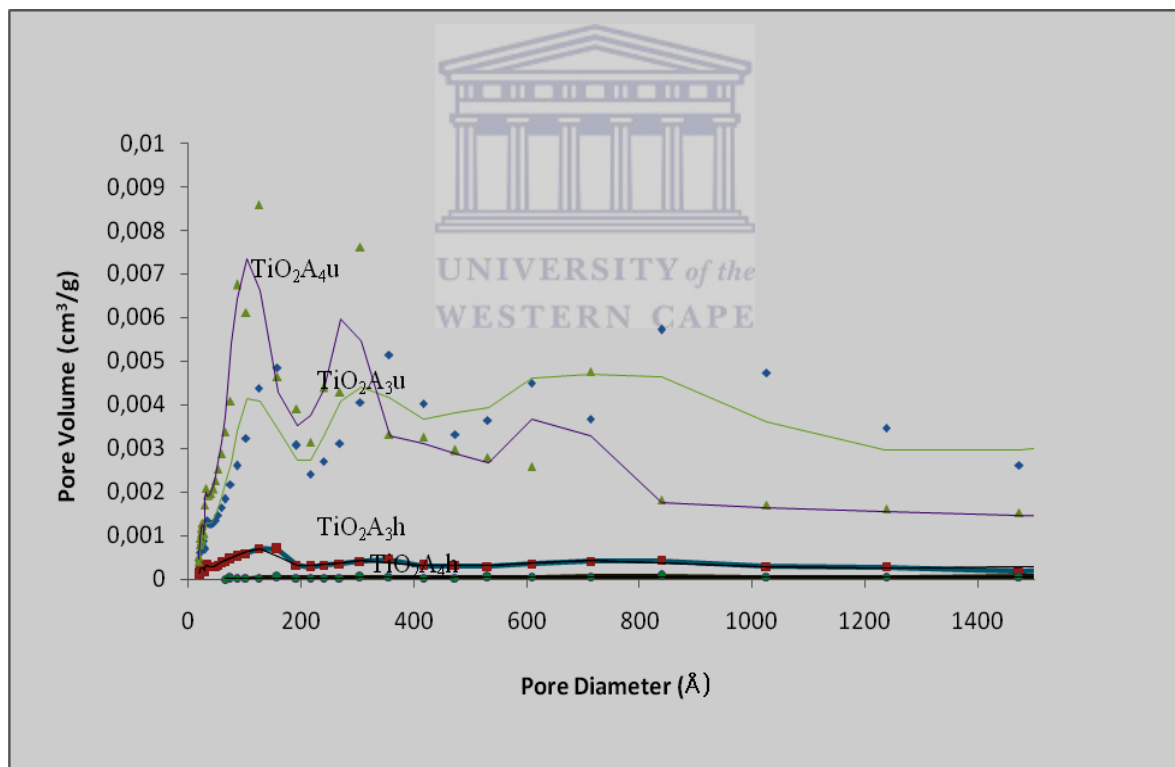
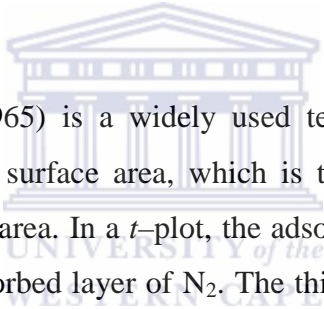


Figure 4.11: Comparison of pore size distribution of (a) TiO_2A_3 (unheated); (b) TiO_2A_3 (heated at 850 °C for 3 h); (c) TiO_2A_4 (90-212 μm , heated); (d) TiO_2A_4 (90-212 μm , heated) (External source: University of Cape Town measurement facility)

A detailed comparison between pore size distributions from N₂ adsorptions for the unheated TiO₂ samples indicated broadly similar modal mesopore sizes and pore size ranges however the heated samples show very low mesoporosity. The data from the unheated TiO₂ sources also showed higher pore volume and therefore higher profiles (Figure 4.11). On the contrary, the heated TiO₂ samples showed lower pore volumes and the peak for the TiO₂A₄h sample at higher pore-size is missing. Additionally, the pore diameters of all the samples were in the range of 0 - 20 nm calculated by the BJH adsorption of size distribution. In each case, the dominant pore modes remained the same but the differential pore volume for each pore-size differed significantly, particularly for the unheated samples. The PSD profiles from N₂ gas adsorptions (Figure 4.11) suggest that pore diameter distribution emphasizes the benefits of no heat treatment, even though, compositionally the samples contain the same chemical contents. The higher measured pore volume in the unheated samples by N₂ gas adsorption techniques indicates that these samples have a significant volume of small pores with <20 nm pore-size.

The logo of the University of the Western Cape, featuring a classical building facade with columns and a pediment, with the text 'UNIVERSITY of the WESTERN CAPE' below it.
T-plot (Lippens & De Boer, 1965) is a widely used technique to estimate the specific micropore volume and the open surface area, which is the surface area from mesopores, macropores, and external surface area. In a *t*-plot, the adsorbed N₂ volume is plotted against statistical thickness (*t*) of the adsorbed layer of N₂. The thickness (*t*) depends on the relative pressure (*P/P*₀). Webb & Orr (1997) write that if the *V* vs. *t* plot yields a straight line that passes through the origin, then the sample is considered to be free of micropores and *t*-plot of microporous material shows a straight line at medium *t* and a concave-down curve at low *t*. Results of *t*-plots from the four TiO₂ samples are presented in Figure 4.12 for comparison.

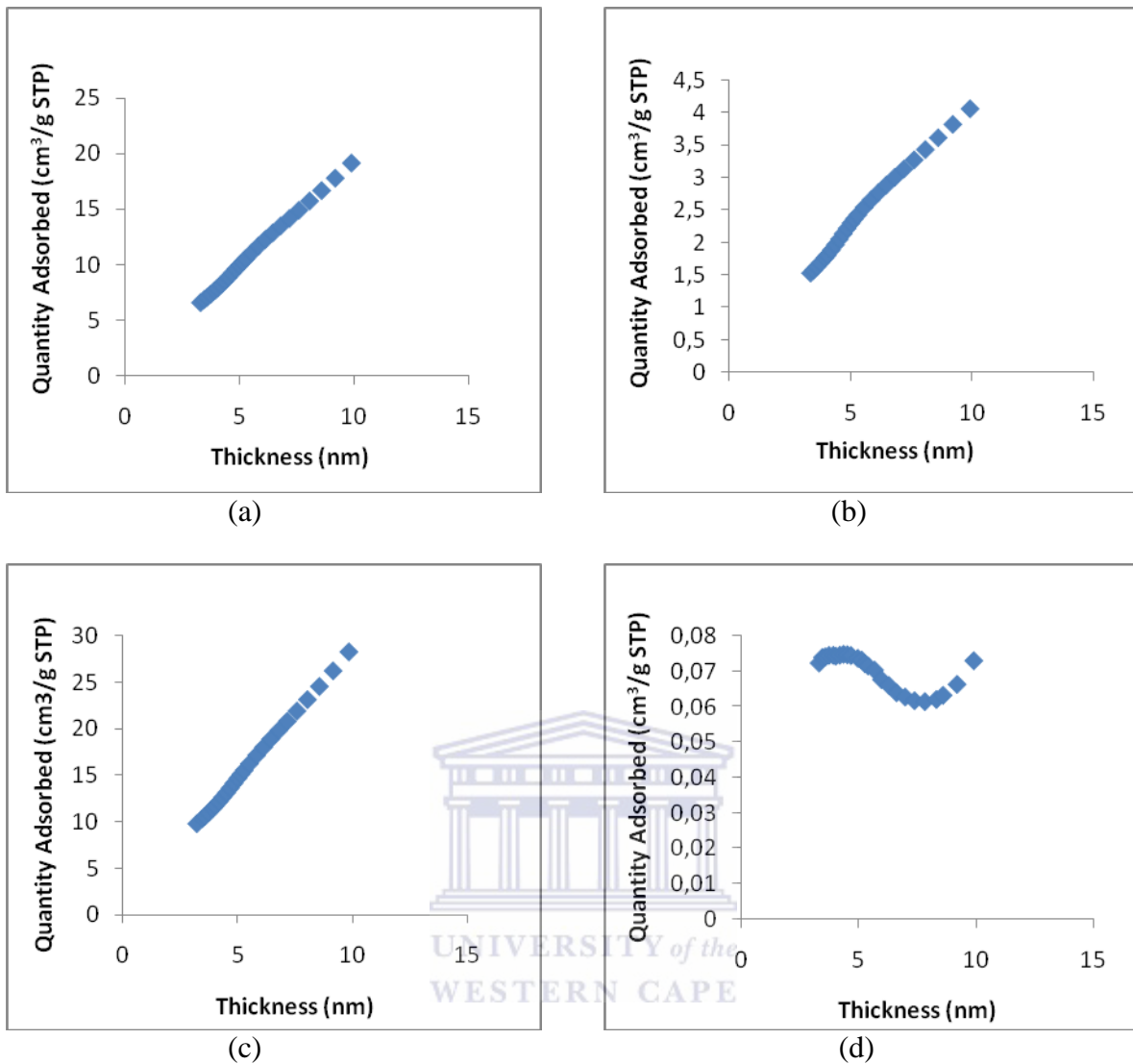


Figure 4.12: T-plot curves of (a) TiO_2A_3 (unheated); (b) TiO_2A_3 (heated at $850\text{ }^\circ\text{C}$ for 3 h); (c) TiO_2A_4 (90-212 μm , heated); (d) TiO_2A_4 (90-212 μm , heated) (External source: University of Cape Town measurement facility)

From the t-plot curves it was possible to estimate the volume of the micropores of all the TiO_2 sources. The first thing to note about the N_2 sorption isotherms is the significant differences in the volumes adsorbed by the samples during the adsorption process. The unheated TiO_2A_3 and TiO_2A_4 sources samples have a very high pore volume of 20 and 30 cm^3/g STP, respectively, compared to the heated samples. The heated TiO_2A_4 has an exceptionally low volume of micropores compared to the pore volumes measured in the heated TiO_2A_3 (Figure 4.12(d)). The extremely low porosity and adsorption of these samples are consistent with the pore size diameter results obtained (Figure 4.11). The N_2 sorption isotherms at $-196\text{ }^\circ\text{C}$ showed a similar trend where the heated samples revealed absence of

open micropore and mesopores (Figure 4.9 and 4.10) and extremely low surface area and pore volume. The dominance of 4–12 nm pores in these samples (Figure 4.12) correlate well with presence of pores of $<200 \text{ \AA}$ diameters (Figure 4.11).

It is demonstrated in this study that detailed and qualitative descriptions of the TiO_2 porosity can provide detailed pore–structure quantification. The understanding of the N_2 gas adsorption technique to understand the pore–structures can aid in modelling a cation exchange capacity during sample preparation with significant production implications. The studies conclusively indicated that unheated TiO_2A_3 and TiO_2A_4 samples can be used for $^{68}\text{Ge}/^{68}\text{Ga}$ generator applications without any heat applied to the sorbents. By omitting heat treatment of the TiO_2 sample powders, the sample preparation became easier and quicker compared with that in earlier literatures. Adsorptive capacity of solids absorbents generally is proportional to the specific surface area. Overall, this work provided a much-needed framework for a good study design before data collection began. TiO_2A_4 , as shown in the results of experimental section 3.4.1, has lower particle size than TiO_2A_3 , which makes the former an ideal raw material for the production of $^{68}\text{Ge}/^{68}\text{Ga}$ generators, without additional heating steps.

4.7 ^{68}Ge Loading Conditions using the various commercial TiO_2 sources

The five commercially available TiO_2 metal oxide materials, TiO_2A_0 (Experiment 1-9), TiO_2A_1 (Experiment 10-13), TiO_2A_2 (Experiment 14-17), TiO_2A_3 (Experiment 18-21) and TiO_2A_4 (Experiment 22-25) that were evaluated for their absorption of ^{68}Ge and desorption of ^{68}Ga are shown in Tables 4.5 (TiO_2A_0) to Table 4.9 (TiO_2A_4). The experimental procedures for the five various sources of the TiO_2 metal oxide are detailed in section 3.2., where n is the number of observations in the original sample.

Table 4.5: ^{68}Ge retention using STMI $\text{TiO}_2 \cdot x\text{H}_2\text{O}$ (TiO_2A_0) metal oxide in 0.005 M and 0.1 M HCl (n=3)

Exp.	Type of metal oxide	Particle size (μm)	Temp. ($^{\circ}\text{C}$)	^{68}Ge loaded (mCi)	HCl (M)	^{68}Ge Retained (%)	^{68}Ga Eluted (%)
1	$\text{TiO}_2\text{A}_0\text{u}150$	90-150	No heat	5.221	0.005	70	46
2	$\text{TiO}_2\text{A}_0\text{u}212$	90-212	No heat	5.115	0.005	80	40
3	$\text{TiO}_2\text{A}_0\text{u}>212$	>212	No heat	3.352	0.005	100	34
4	$\text{TiO}_2\text{A}_0\text{u}150$	90-150	No heat	3.022	0.1	41	28
5	$\text{TiO}_2\text{A}_0\text{h}150$	90-150	850	3.118	0.1	21	4
6	$\text{TiO}_2\text{A}_0\text{u}212$	90-212	No heat	4.251	0.1	71	26
7	$\text{TiO}_2\text{A}_0\text{h}212$	90-212	850	4.227	0.1	60	50
8	$\text{TiO}_2\text{A}_0\text{u}>212$	>212	No heat	3.188	0.1	80	5
9	$\text{TiO}_2\text{A}_0\text{h}>212$	>212	850	3.210	0.1	65	25

In experiment 1, when a particle size fraction of 90-150 μm ($\text{TiO}_2\text{A}_0\text{u}150$) was used to load ^{68}Ge in a 0.005 M HCl media, 70% of the ^{68}Ge radionuclide managed to adsorb on the TiO_2 , suggesting a 30% loss. When the same metal oxide (90-150 μm , $\text{TiO}_2\text{A}_0\text{u}150$) was investigated under the same conditions, with acid media changed to 0.1 M HCl (Experiment 5), the yield decreased to 41%. This indicated a loss of 59% of the ^{68}Ge , which could be attributed to the high acid content of the eluate. Overall the 90-150 μm ($\text{TiO}_2\text{A}_0\text{u}150$) size was rejected due to low ^{68}Ge retention.

In experiment 2, when a particle size fraction of 90-212 μm ($\text{TiO}_2\text{A}_0\text{u}212$) was used to load ^{68}Ge in a 0.005 M HCl media, the yield increased to 80%. Again, 20% of the ^{68}Ge was lost and this suggested further analysis of the metal oxide. For the same metal oxide, when using 0.1 M HCl media (experiment 6), the yield was decreased to 71%, a decline when the acid concentration was increased. Therefore, the 90-212 μm ($\text{TiO}_2\text{A}_0\text{u}212$) was discarded.

In experiment 3, when a particle size fraction of >212 μm ($\text{TiO}_2\text{A}_0\text{u}>212$) was used to load ^{68}Ge in a 0.005 M HCl media, the yield was 100%, suggesting a zero loss. For the first time, a 100% loading of ^{68}Ge was achieved when a >212 μm particle size fraction was used when loading ^{68}Ge in a 0.005 M HCl media. Again, when the same metal oxide (>212 μm ($\text{TiO}_2\text{A}_0\text{u}>212$)) was used in experiment 8, this time changing the ^{68}Ge media to 0.1 M HCl, the yield was reduced to 80%. The two experiments (3 and 8) suggested that the optimum eluent was 0.005 M HCl rather than 0.1 M HCl when >212 μm size ($\text{TiO}_2\text{A}_0\text{u}>212$) was used as a sorbent.

In experiment 4, when a particle size fraction of 90-150 μm ($\text{TiO}_2\text{A}_0\text{u}150$) was used to load ^{68}Ge and compared to experiment 6, when 90-212 μm ($\text{TiO}_2\text{A}_0\text{u}212$) was used to load ^{68}Ge , with both experiments using 0.1 M HCl media, the yield increased from a retention of 41% for the 90-150 μm ($\text{TiO}_2\text{A}_0\text{u}150$) to a retention of 71% for the 90-212 μm ($\text{TiO}_2\text{A}_0\text{u}212$). The comparison suggested that a bigger particle size was more appropriate for good retention, in this case 90-212 μm ($\text{TiO}_2\text{A}_0\text{u}212$). In experiment 8 and 9, in which case both experiments used >200 μm ($\text{TiO}_2\text{A}_0\text{u}>212$) to load ^{68}Ge , except that in one case (experiment 9, >212 μm ($\text{TiO}_2\text{A}_0\text{h}>212$)) the metal oxide was heated to 850 C for 3 hours, the ^{68}Ge yield was found to be 80% for the unheated >212 μm ($\text{TiO}_2\text{A}_0\text{u}>212$) and 65% for the heated >212 μm ($\text{TiO}_2\text{A}_0\text{h}>212$). Again, the comparison in this case suggested that heat treatment did not improve the loading of the ^{68}Ge radionuclide. In experiment 6 and 7, when 90-212 μm ($\text{TiO}_2\text{A}_0\text{u}212$) particle size was used to load ^{68}Ge in 0.1 M HCl for both experiments, (with heat-treatment as the only factor added to experiment 7), the retention of the ^{68}Ge was found to be 71% or 60% for the unheated or heated $\text{TiO}_2\text{A}_0\text{h}212$, respectively. As before, the experiments (6 and 7) suggested that heat-treatment when using the STMI product did not contribute positively to the retention of the ^{68}Ge radionuclide.

In summary, in the first 3 experimental runs, when using the TiO_2A_0 (STMI oxtain) in the 0.005 M HCl eluent, 100% retention of ^{68}Ge could be ideally achieved on a sample with a particle size >212 . Also, it was shown, when starting with a 0.005 M HCl eluent as shown in experimental runs 1-4 that, as the particle size increased with no heat, the retention of ^{68}Ge increased from 70% (90-150 μm), to 80% (90-212 μm) and 100% (>212 μm). It was furthermore shown that as the particle size of the TiO_2A_0 increased with heating at 850 $^\circ\text{C}$ that retention of ^{68}Ge was only 21% (90-150 μm), 60% (90-212 μm) and 65% (>212 μm). When the TiO_2A_0 was not heated, improved retention of the ^{68}Ge with increasing particle size (90-150 μm , a retention of 41%), and 90-212 μm with a retention of 71% and >212 μm with a retention of 80% was evident, but this was still not adequate for the generator requirements. The optimal experimental conditions were obtained in run 3 when using the TiO_2A_0 with a particle size of >212 μm , with no heating and in 0.005 M HCl matrix, where retention of 100% ^{68}Ge was achieved. In the end, the initial experiments (Experiment 1-9) involving TiO_2A_0 proved to be unsuccessful, as STMI stopped producing its TiO_2 on a commercial basis and therefore no further investigations were pursued with this TiO_2 compound. Another

disadvantage of the product was that while the 100% loading (Experiment 3) was impressive, no ^{68}Ge was found in the eluate when elution with 10 ml of the 0.005 M HCl was performed.

Subsequent experiments were performed using TiO_2A_1 (Sigma-Aldrich) and TiO_2A_2 (Alpha-Aesar). Table 4.6 and Table 4.7 present the HCl concentration and the temperature dependence of the TiO_2A_1 and TiO_2A_2 , respectively for ^{68}Ge retention. The samples were sieved into two size fractions (90-212 or 212-300 μm). Again, n is the number of observations in the original sample.

Table 4.6: ^{68}Ge retention of the TiO_2A_1 with 0.005 M and 0.1 M HCl (n=3)

Exp.	Type of metal oxide	Particle size (μm)	Temp. ($^\circ\text{C}$)	^{68}Ge loaded (mCi)	HCl (M)	^{68}Ge Retained (%)
10	$\text{TiO}_2\text{A}_1\text{u}212$	90-212	No heat	1.002	0.005	0
11	$\text{TiO}_2\text{A}_1\text{h}212$	90-212	850	1.254	0.005	0
12	$\text{TiO}_2\text{A}_1\text{u}300$	212-300	No heat	1.145	0.1	0
13	$\text{TiO}_2\text{A}_1\text{h}300$	212-300	850	1.335	0.1	0

Table 4.7: ^{68}Ge retention of the TiO_2A_2 with 0.005 M and 0.1 M HCl (n=3)

Exp.	Type of metal oxide	Particle size (μm)	Temp. ($^\circ\text{C}$)	^{68}Ge loaded (mCi)	HCl (M)	^{68}Ge Retained (%)
14	$\text{TiO}_2\text{A}_2\text{u}212$	90-212	No heat	1.021	0.005	0
15	$\text{TiO}_2\text{A}_2\text{h}212$	90-212	400	1.115	0.005	0
16	$\text{TiO}_2\text{A}_2\text{u}300$	212-300	No heat	1.251	0.1	0
17	$\text{TiO}_2\text{A}_2\text{h}300$	212-300	400	1.362	0.1	0

In experiment 10-13 (Table 4.6), when a particle size fraction of 90-212 or 212-300 μm of the TiO_2A_1 from Sigma-Adrich were used to load the ^{68}Ge in either 0.005 or 0.1 M HCl media, the yield obtained revealed that no ^{68}Ge was retained by the TiO_2A_1 , irrespective of the temperature or the particle size used. Therefore, the use of TiO_2A_1 as a sorbent was rejected due to zero percent loading of the ^{68}Ge . Similarly, in experiment 14-17 (Table 4.7), when 90-212 and 212-300 μm of the TiO_2A_2 were used to load the ^{68}Ge in either 0.005 or 0.1

M HCl media, once again, the yield obtained revealed that no ^{68}Ge was retained by the TiO_2A_2 , irrespective of the temperature or the particle size used. As before, the use of TiO_2A_2 as a sorbent was rejected due to zero percent loading of the ^{68}Ge . No ^{68}Ga elution was performed for both sources (TiO_2A_1 and TiO_2A_2) due to zero amount of ^{68}Ge loaded onto the column.

Thereafter, different kinds of TiO_2 were investigated in order to find conditions where the metal oxide material could load ^{68}Ge effectively, and, thereafter, release the ^{68}Ga . It was thus decided to purchase the TiO_2A_3 and TiO_2A_4 powders from Evonik Industries. Table 4.8 and 4.9 represent the results of the Evonik samples TiO_2A_3 and TiO_2A_4 , where approximately 1 mCi of the ^{68}Ge was used for loading.

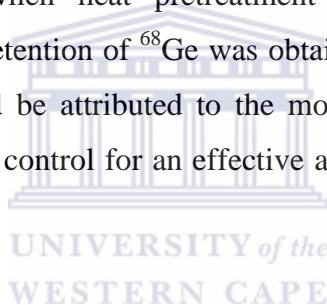
Table 4.8: ^{68}Ge retention of the TiO_2A_3 with 0.005 M HCl and 0.1 M HCl (n=3)

Exp.	Type of metal oxide	Particle size (μm)	Temp. ($^{\circ}\text{C}$)	^{68}Ge loaded (mCi)	HCl (M)	^{68}Ge Retained (%)	^{68}Ga Eluted (%)
18	$\text{TiO}_2\text{A}_3\text{u}$	No Sieving	No Heat	0.998	0.005	100	20
19	$\text{TiO}_2\text{A}_3\text{h}$	No Sieving	850	1.042	0.005	40	62
20	$\text{TiO}_2\text{A}_3\text{h}$	No Sieving	850	1.140	0.1	50	40
21	$\text{TiO}_2\text{A}_3\text{u}$	No Sieving	No heat	1.244	0.1	100	45

Table 4.9: ⁶⁸Ge retention of the TiO₂A₄ with 0.005 M HCl and 0.1 M HCl (n=3)

Exp.	Type of metal oxide	Particle size (µm)	Temp. (°C)	⁶⁸ Ge loaded (mCi)	HCl (M)	⁶⁸ Ge Retained (%)	⁶⁸ Ga Eluted (%)
22	TiO ₂ A ₄ u300	212-300	No heat	1.118	0.005	60	39
23	TiO ₂ A ₄ h212	90-212	850	1.555	0.005	30	24
24	TiO ₂ A ₄ u212	90-212	No heat	1.612	0.1	100	54
25	TiO ₂ A ₄ h300	212-300	850	1.624	0.1	35	35

When using these TiO₂ sources (Table 4.8 and Table 4.9), the use of 0.005 M HCl as eluent of ⁶⁸Ga was immediately rejected albeit impressive loading results (Experiment 18, 21 and 22), as there was massive breakthrough of ⁶⁸Ge, thereby, disqualifying the use of this method. The use of TiO₂A₄ with heat treatment (850 °C, 3 hours) showed retention of the ⁶⁸Ge of 50% with the 0.1 M HCl eluate (Experiment 20) and 40% in the 0.005 M HCl eluate (Experimental 19). However when heat pretreatment was not used on the TiO₂A₄ (Experiment 18 and 21), 100% retention of ⁶⁸Ge was obtained with both the 0.1 M HCl and 0.005 M HCl eluent. This could be attributed to the morphology and particle size of the TiO₂A₃, two important factors to control for an effective application of the TiO₂ powders as ⁶⁸Ge/⁶⁸Ga generator sorbents.



Because heat treatment of the sample increased particle size (see Table 4.1) and simultaneously reduced the surface area, the untreated TiO₂A₃ and TiO₂A₄ sample (Experiment 18, 21 and 24) showed higher adsorption of ⁶⁸Ge of 100%. While, on the other hand, the untreated sample showed adsorption of ⁶⁸Ge of 60% (Experiment 22). Additionally, a particle size of 90-212 µm meant a reduced particle size when compared to a particle size of 212-300 µm (Experiment 22-25); this in turn, implied an increased surface area. The improved ⁶⁸Ge retention observed for experiment 24 could be attributed to the more theoretical plates that could be available with the smaller particle size (90-212 µm) TiO₂A₄ compared to the larger particle size (212-300 µm). Because of this reason, the particle size fraction of 212-300 µm obtained much lower ⁶⁸Ge adsorption when compared to 90-212 µm. Experiment 23 and 25 showed low ⁶⁸Ge adsorption due to bigger particle size which played a more significant role than the heat treatment. From the results, it was deduced that the anatase form of TiO₂ and a smaller particle size are essential for effective ⁶⁸Ge adsorption.

4.8 ⁶⁸Ga Elution and ⁶⁸Ge Breakthrough Analysis

Of the five TiO₂ metal oxides investigated, the TiO₂A₀ (>212 μm, unheated, 0.005 M HCl), TiO₂A₃ (heated, 0.1 M and 0.005 M HCl) and TiO₂A₄ (90-212 μm, unheated, 0.1 M HCl), showed 100% retention of ⁶⁸Ge. Both the Sigma Aldrich TiO₂ (TiO₂A₁ and TiO₂A₂) showed no retention of ⁶⁸Ge at the particle size or treatment evaluated. During the course of the investigations, STMI stopped producing its TiO₂ on a commercial basis and therefore no further investigations were pursued with this TiO₂ source. The TiO₂A₃ (850°C, 0.1 M or 0.005 M HCl) and TiO₂A₄ (90-212 μm, unheated, 0.1 M HCl), was therefore pursued for further investigations as set out in Table 4.10. Table 4.10 represents the results of the TiO₂A₃ and TiO₂A₄ after each metal oxide was loaded with approximately 15 mCi ⁶⁸Ge in 0.1 M HCl. Again, *n* is the number of observations in the original sample.

Table 4.10: ⁶⁸Ge retention and ⁶⁸Ga desorption of the TiO₂A₃ and TiO₂A₄ with 0.1 M HCl (n=3)

Exp.	Type of metal oxide	Particle size (μm)	Temp. (°C)	⁶⁸ Ge loaded (mCi)	HCl (M)	⁶⁸ Ge Retained (%)	⁶⁸ Ga Elution (%)
26	TiO ₂ A ₃ u	No Sieving	No heat	15.225	0.1	100	45
27	TiO ₂ A ₄ h212	90-212	No heat	15.448	0.1	100	54

A 15 mCi TiO₂A₃ based ⁶⁸Ge/⁶⁸Ga generator and TiO₂A₄ based ⁶⁸Ge/⁶⁸Ga generator system, prepared as described in Chapter 3, section 3.2 (Experiment 26 and 27), were evaluated over a 12 month period and results are shown in Figures 4.13 to Figure 4.16.

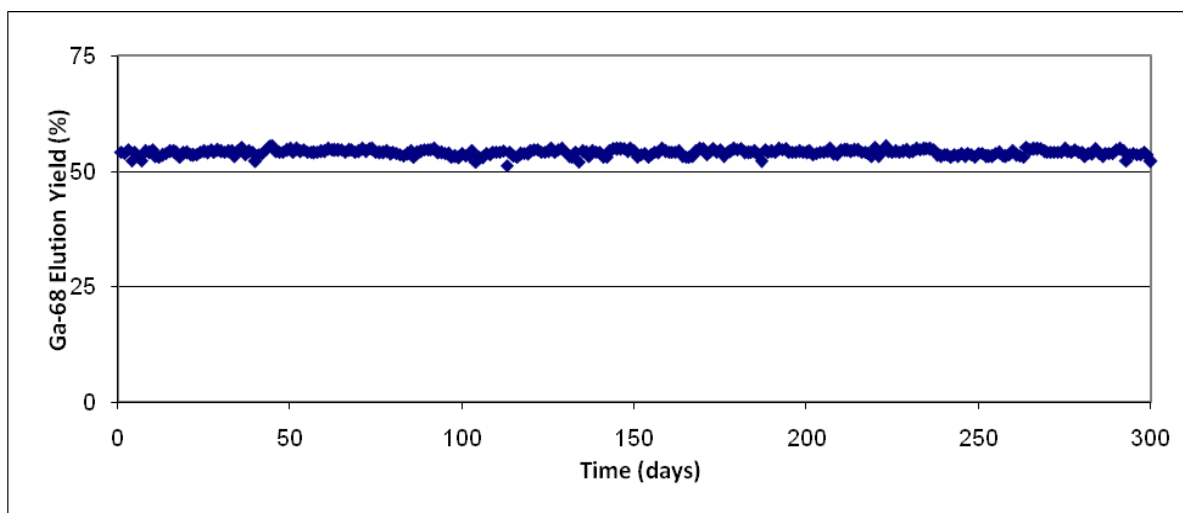


Figure 4.13: Elution Efficiency of ^{68}Ga of TiO_2A_4 in 0.1 M HCl (column: 3 mm i.d. x 30 mm length; sorbent: 3 g TiO_2A_4 ; ^{68}Ge loaded onto the column: 15 mCi; eluent: 0.1 M HCl)

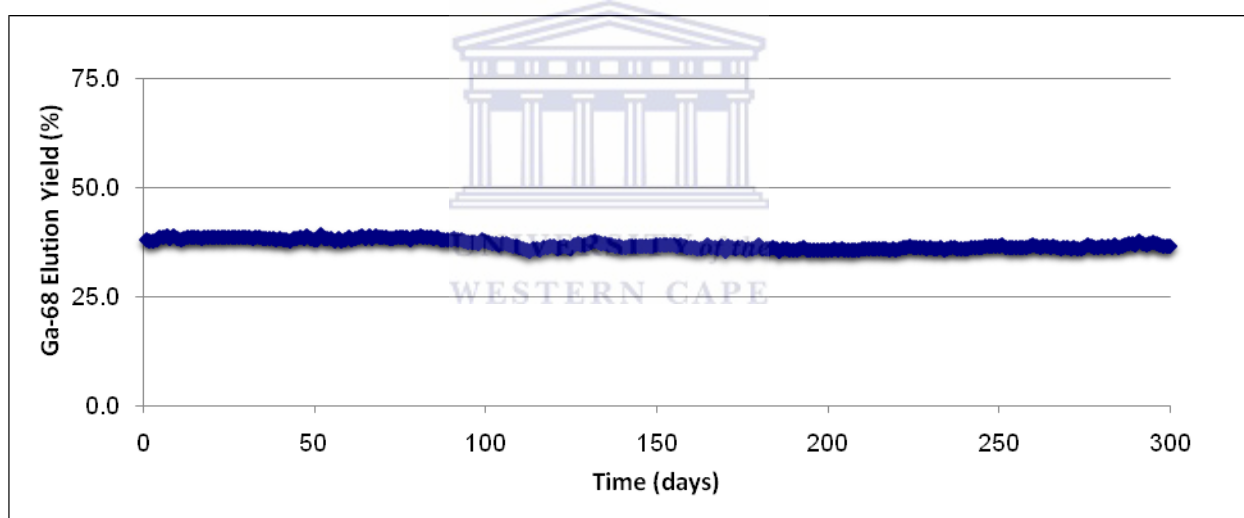


Figure 4.14: Elution Efficiency of ^{68}Ga TiO_2A_3 in 0.1 M HCl (column: 3 mm i.d. x 30 mm length; sorbent: 3 g TiO_2A_3 ; ^{68}Ge loaded onto the column: 15 mCi; eluent: 0.1 M HCl)

Figure 4.13 shows the ^{68}Ga elution curve of the TiO_2A_4 based $^{68}\text{Ge}/^{68}\text{Ga}$ generator showing a consistent yield of 54% at over 300 elutions and Figure 4.14 shows the ^{68}Ga elution curve of TiO_2A_3 , which yielded 40% ^{68}Ga over 300 elutions. For both these TiO_2 samples evaluated, the ^{68}Ga elution curves appeared relatively stable throughout the 300 elutions, displaying good stability and no physical degradation over the more than 12 month period.

The immediate difference between the two TiO_2 metal oxides (TiO_2A_3 and TiO_2A_4) could be seen in the intensity of the peaks when XRD as well as the images generated by SEM and TEM technique were analyzed, which revealed the crystallite size and crystallinity, respectively. The peaks of the TiO_2A_3 metal oxide were higher, indicating a larger crystallite size, with higher overall crystallinity, while the peaks of the TiO_2A_4 metal oxide were smaller, sharper and more defined, representing larger, more uniform crystallite in terms of size and distribution. Therefore, the higher ^{68}Ga elution of TiO_2A_4 metal oxide compared to the TiO_2A_3 may be associated with three key parameters: smaller particle size, no heat treatment and high anatase content. The use of a heat treatment to preheat the TiO_2A_3 had a negative effect on the surface area. Breakthrough of ^{68}Ge was determined 24 hours after elution (see Experiment 3.3.2), using 50 cm distance at which the ^{68}Ge detector was calibrated. After a period of 12 months, the ^{68}Ga generator was still performing well, with no visible sign of breakthrough of ^{68}Ge or metal oxide discolouration. As shown in Figure 4.15 and Figure 4.16, the ^{68}Ge breakthrough for the TiO_2A_4 metal oxide for over 300 elutions was averaging at about 0.05% compared to less than 0.05% for the TiO_2A_3 metal oxide. This implied that, even though the ^{68}Ga efficiency for the TiO_2A_4 was above 50% mark, more work needed to be done in order to improve the ^{68}Ge breakthrough.

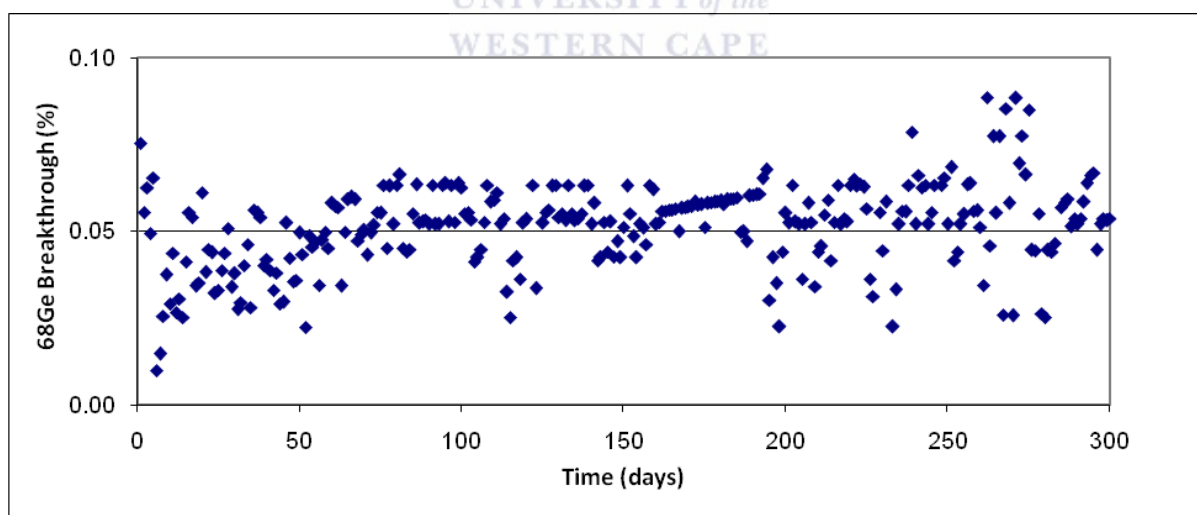


Figure 4.15: ^{68}Ge breakthrough of TiO_2A_4 in 0.1 M HCl (column: 3 mm i.d. x 30 mm length; sorbent: 3 g TiO_2A_4 ; ^{68}Ge loaded onto the column: 15 mCi; eluent: 0.1 M HCl)

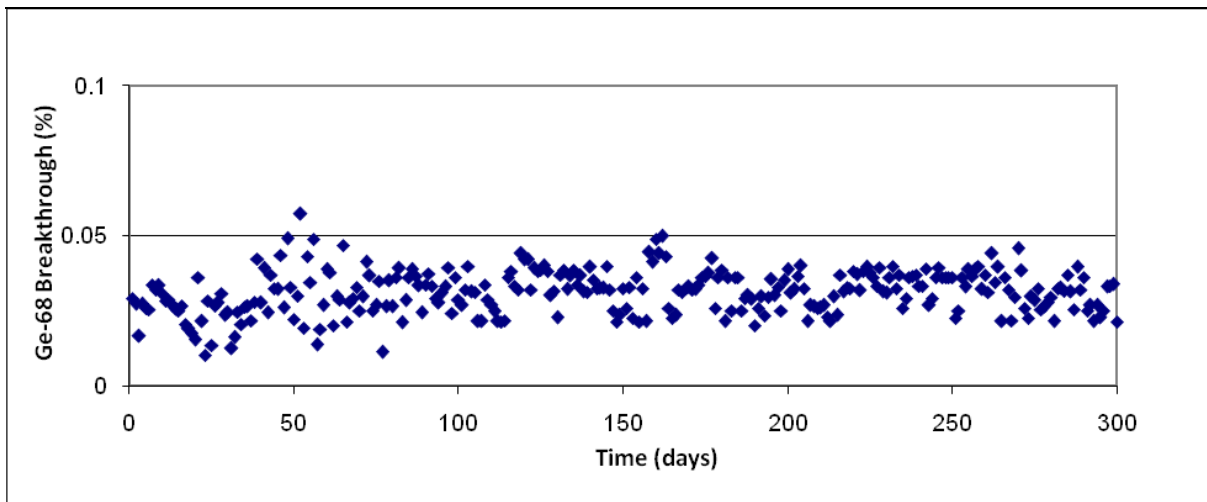


Figure 4.16: ^{68}Ge breakthrough of TiO_2A_3 in 0.1 M HCl (column: 3 mm i.d. x 30 mm length; sorbent: 3 g TiO_2A_3 ; ^{68}Ge loaded onto the column: 15 mCi; eluent: 0.1 M HCl)

Because of the superior ^{68}Ga elution of above 50%, further investigations were limited to the TiO_2A_4 based $^{68}\text{Ge}/^{68}\text{Ga}$ generator. On the other hand, the ^{68}Ge breakthrough of the TiO_2A_4 metal oxide implied that more work was required for the improvement of this limitation.

Figure 4.17 shows the elution profile of the ^{68}Ga of the TiO_2A_4 based $^{68}\text{Ge}/^{68}\text{Ga}$ generator where it was shown that generally >95% of the ^{68}Ga was eluted in the first 6-7 ml and >80% of the ^{68}Ga could be found in a single 6 ml fraction.

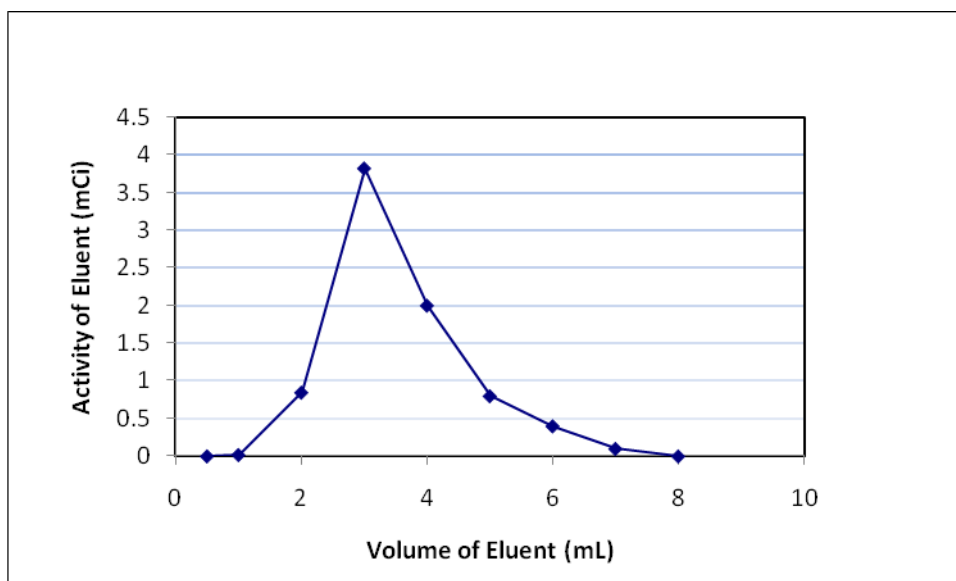


Figure 4.17: ⁶⁸Ga Elution Profile of the TiO₂A₃ metal oxide (column: 3 mm i.d. x 30 mm length; sorbent: 3 g TiO₂A₄; ⁶⁸Ge loaded onto the column: 15 mCi; eluent: 0.1 M HCl)

The elution profile step, as explained in Section 3.2 (Experiment 28), was performed to recover the maximum amount of ⁶⁸Ga in the minimal volume of 0.1 M HCl from the ⁶⁸Ge generator eluate. The elution profile of the ⁶⁸Ga from the TiO₂A₄ metal oxide shows the highest elution in the first 4 ml 0.1 M HCl fraction, i.e. >80% in fraction # 1-5 and >10% in fraction # 5-6. Altogether, about 95% of ⁶⁸Ga were being successively eluted in only 6 ml of HCl. This implied that a smaller elution volume was required in order to elute the sorbed ⁶⁸Ga. This is a ⁶⁸Ge/⁶⁸Ga generator requirement as it leads to a short chemical separation process and can be an important factor in the final product as the yield is dependent on the half-life of a specific radionuclide. It would also minimize the quantities of waste solutions being generated (which are normally radioactive, should the separation involve radioactivity), which are monitored and, normally, have to be stored for a period of time before being released to waste storage dams on site.

4.9 ⁶⁸Ga Eluate Metal Analysis

Table 4.11 represents the results of analysis for the determination of the elemental composition of the eluate using the TiO₂A₄ source. The analytical curves for the Zn, Fe, Sn, Ti, Cu, Al, Ga and Ge were done according to the procedure described in the experimental part (3.4.6). The curves are shown in Appendix B. The analysis was for Zn, Fe, Sn, Ti, Cu,

Al, Ga and Ge determinations in the several ^{68}Ga eluate samples over a period of 12 months. The results are described in Table 4.10. As before, n is the number of observations in the original sample.

Table 4.11: Random metal analysis of ^{68}Ga eluate of the TiO_2A_4 (ppm) (n=3)

Run No.	Zn	Fe	Sn	Ti	Cu	Al	Ga	Ge
1	<1	<1	<1	<1	<1	<1	<1	<1
2	<1	<1	<1	<1	<1	<1	<1	<1
3	<1	<1	<1	<1	<1	<1	<1	<1
4	<1	<1	<1	<1	<1	<1	<1	<1
5	<1	<1	<1	<1	<1	<1	<1	<1
6	<2	<1	<1	<1	<1	<1	<1	<1
7	<1	<1	<1	<1	<1	<1	<1	<1
8	<1	<1	<1	<1	<1	<1	<1	<1
9	<1	<1	<1	<1	<1	<1	<1	<1
10	<1	<1	<1	<1	<1	<1	<1	<1
11	<1	<1	<1	<1	<1	<1	<1	<1
12	<1	<1	<1	<1	<1	<1	<1	<1

The results of Table 4.11 demonstrated that random metal analysis of the 300 daily elutions (eluate) of the TiO_2A_4 had shown that the metal ion impurities of Zn, Fe, Sn, Ti, Cu, Al, Ga and Ge, were found to be <1 ppm for each metal. This was an important requirement as any chemical impurities in the ^{68}Ga eluate would interfere in the complexation of ^{68}Ga with the various ligands and biomolecules. As was pointed out in the introduction to this study in chapter 1, section 1.3, high metallic impurities would adversely affect the ^{68}Ga labelling yields as well as the activity of the labelled product. The regular analysis of ^{68}Ga eluates for a range of metals, i.e. Zn, Fe, Sn, Ti, Cu, Al, Ga and Ge, was carried out and any sudden change in concentration of a particular metal would have indicated a defect before the TiO_2 based $^{68}\text{Ge}/^{68}\text{Ga}$ generator fails completely.

4.10 Chapter Summary

In this chapter, a $^{68}\text{Ge}/^{68}\text{Ga}$ radionuclide generator based on an inorganic cation exchange mechanism on a titanium oxide (TiO_2) is presented. A more detailed description of $^{68}\text{Ge}/^{68}\text{Ga}$ generators is given in Chapter 2. In a first approach, the determination of adsorption parameters by the various TiO_2 sources was investigated in batch studies. In a second approach, characterization studies (XRD, XRF, SEM and TEM) of the supplied TiO_2 samples

were performed to better understand parameters such as particle size, morphology as well as chemical composition. In a third approach, the effectiveness of any TiO₂ source relies on the ⁶⁸Ga radioactivity produced, ⁶⁸Ge breakthrough and metallic ion contamination of the ⁶⁸Ga eluate. Quality assessment and operational performance evaluation were carried out in order to determine the difference between the TiO₂ sources on the required properties of a ⁶⁸Ge/⁶⁸Ga generator. Unfortunately, during this time STMI stopped production of the oxitan TiO₂ used for initial experiments, before any valuable information could be gained from the STMI TiO₂ metal oxide. In the literature, several examples of metal oxides were presented, that could, instead, be used for the ⁶⁸Ge adsorption; however, due to time constraints it was opted to only pursue commercially available TiO₂ compounds. As a result, Sigma-Aldrich and Alfa-Aesar TiO₂ in anatase and rutile form as well as Aeroxide® and Aerolyst® sourced from Evonik TiO₂ powders were then investigated. Unfortunately, the experiments involving anatase and rutile form had to be abandoned due to a low ⁶⁸Ge adsorption displayed by both sorbents.

With complete understanding of the principle of ⁶⁸Ge loading of the two sorbents (Aeroxide® and Aerolyst® sources from Evonik), it was possible to carry out ⁶⁸Ga elution performance and ⁶⁸Ge breakthrough and its evaluation. Excellent results were obtained when both Aeroxide® and Aerolyst® sources from Evonik TiO₂ powders were investigated. When the Aerolyst® source was used, more than 50% of the ⁶⁸Ga radioactivity was eluted in 5 ml 0.1 M HCl solution over a period of 12 months. On the other hand, when the Aeroxide® was used, more than 40% of the ⁶⁸Ga radioactivity was eluted in 5 ml 0.1 M HCl solution over the same period of time. The long half-life of the ⁶⁸Ge provided long operating lifetime of the ⁶⁸Ga generator. The regular analysis of the ⁶⁸Ga eluate for a range of quality control parameters (⁶⁸Ga efficiency, ⁶⁸Ge breakthrough and metal contaminants) was carried out and any sudden change in these response parameters would have indicated a wear of the column before the TiO₂ source fails completely. Finally, analysis of the metal contaminants followed.

Based on the encouraging results from the preliminary experiments, a study was performed using Aeroxide® and Aerolyst® (Evonik Industries) TiO₂ powders (TiO₂A₃ and TiO₂A₄). In the case of the Aeroxide® (TiO₂A₃), the optimum parameters (100% load with 0.1 M HCl) for the ⁶⁸Ge loading were found to be: 3 g, unsieved, 850 °C for 3 h. Again, in the case of the

Aerolyst®, the optimum parameters were found to be: 3 g, 90-212 µm and no heat treatment. The elution yield of the TiO₂A₃ and TiO₂A₄ were found to be 45 and 54%, respectively. An elution value of less than 60% indicates poor yield. Such low value was the result of HCl concentration (0.1 M) which had to be unchanged due to labeling studies which uses this acid strength as means of elution medium. The ⁶⁸Ge breakthrough in the ⁶⁸Ga eluate from the TiO₂A₄ was low and consistent at 0.05% when compared to that of TiO₂A₃ which was also consistently less than 0.05%. The ⁶⁸Ge breakthrough of the TiO₂A₄ implied that more work had to be done in order to reduce the amount of ⁶⁸Ge co-eluted with ⁶⁸Ga. Morphological characterization was performed to understand characteristics of the samples. X-ray diffraction (XRD) was used to calculate the crystallite size. Scanning Electron Microscopy (SEM) and Transmission Electron Microscopy (TEM) were performed to determine the grain size and particle size, respectively. In almost all the cases, when the particle size was decreased, significant amounts of ⁶⁸Ge could be loaded onto the TiO₂ metal oxides and this was attributed to the large surface area exhibited by the reduced particle size.

The adsorption of nitrogen method for determination of porous structure for the heated and unheated TiO₂A₃ and TiO₂A₄ samples was investigated. Analysis of the shapes of the N₂ isotherms, the amount of the N₂ adsorbed and the relative pressure values, provided useful information about the pore volumes, specific surface areas and pore sizes by means of the solid and gas interactions, which were used to qualitatively predict the types of pores present in the adsorbent. The influence of temperature upon porosity of the TiO₂ sources was studied by BET derived from the isotherms, pore volumes and surface area data of the nitrogen gas. Nitrogen adsorption isotherms of the TiO₂A₃ and TiO₂A₄ were of type I and II, respectively, as mesoporous class in the Brunauer classification. Characteristics of different pore size distribution of the TiO₂ sources under investigation were used to describe the adsorption process. The pore volumes calculated from t-plot were found to be approximately 0 to 4 cm³g⁻¹ for the heated samples and between 20 and 30 cm³g⁻¹ for the unheated samples. The shape of the isotherms changes extremely due to high temperature treatment, an indication of the effect of contracting surface area due to increased particle size during the thermal modification process, which is proved to have an adverse effect on adsorption properties.

The presence of metallic impurities in the ^{68}Ga eluate is highly relevant and can affect the utility of the product. Quantification of the amounts of metallic impurities was done by Inductively Coupled Plasma Optical Emission Spectrometry (ICP-OES) and no impurities were detected during HCl elution of the Aeroxide® and Aerolyst® sourced from Evonik TiO_2 powders.

In conclusion, the objective of the present study, namely to obtain a radiochemically pure ^{68}Ga from a TiO_2 based $^{68}\text{Ge}/^{68}\text{Ga}$ generator in a short a period, was achieved. A number of techniques, in conjunction with production of a $^{68}\text{Ge}/^{68}\text{Ga}$ generator, were used to determine the physico-chemical forms of the TiO_2 sources that allowed the separation of ^{68}Ga from the ^{68}Ge radionuclide. A number of TiO_2 sources are commercially available. The most important commercial TiO_2 source for this study is the Aerolyst® sourced from Evonik TiO_2 powders. This metal oxide has a stable crystallite structure, allowing long-term use of the ^{68}Ga generator; high corrosion resistance, that can otherwise affect the quality of the ^{68}Ga eluate negatively, TiO_2 with a purity of 98% was used, implying fewer impurities found in the TiO_2 source for contamination purposes. Under optimum conditions (eluate concentration, column dimensions, TiO_2 source, amount of TiO_2 used) the ^{68}Ga radionuclide was eluted from the ^{68}Ge generator; and radionuclidic purity aspects needed during radiochemical processing to provide ^{68}Ge eluate of high radionuclidic, radiochemical and chemical purity were achieved.

Chapter Five

CONCLUSION

$^{68}\text{Ge}/^{68}\text{Ga}$ generators serve as a reliable source for the radionuclide ^{68}Ga (half-life = 68 mins) which when coupled to DOTA-peptides is used effectively as a nuclear medicine diagnostic tool for neuro-endocrine tumours. It is becoming increasingly difficult to ignore the attractive and ideal chemical properties of this PET radionuclide. As more PET-CT scanners are installed and commissioned in nuclear medicine departments across the world, the demand for an efficient and commercially available $^{68}\text{Ge}/^{68}\text{Ga}$ generator is increasing. In the past three decades a number of researchers have sought to find an ideal sorbent material for the $^{68}\text{Ge}/^{68}\text{Ga}$ generator which would provide favourable properties for ^{68}Ga efficiency, with minimum ^{68}Ge breakthrough and that would minimize metal impurities found in the eluate over the life span of the generator which is generally 9-12 months.

WESTERN CAPE

Little is known about the conditions necessary for the ^{68}Ge adsorption and it is not clear what factors supports ^{68}Ga desorption. There are several reasons that could affect the retention of ^{68}Ge on the column negatively, for instance, complex chemical, physicochemical, radiochemical processes in the column, mechanical defects and insufficient volume of the eluent. When it comes to TiO_2 sources, different microstructures could lead to different physical properties which, in turn, lead to different applications. This conclusion is supported by the results (Table 4.4 to Table 4.8) of the various TiO_2 sources that were analyzed where the knowledge of microstructure (grain size, crystalline structures, surface composition, etc) was indispensable for understanding the macroscopic behaviour of the TiO_2 sources. In addition, no research that surveyed the surface area, particle size and the morphology of the TiO_2 has been found. The key research question of this study was to determine whether TiO_2 could be used as a sorbent material for the production of a $^{68}\text{Ge}/^{68}\text{Ga}$ generator that could be

used in clinical application. Various types of commercially available TiO₂ were investigated to determine whether these sources of TiO₂ differed in their properties.

As shown in the literature survey, commercially available ⁶⁸Ge/⁶⁸Ga generators have generally used SnO₂ or TiO₂ as the generator column eluate. Kozlova et al., (1970) were the first researchers who produced a TiO₂ based ⁶⁸Ge/⁶⁸Ga where 3 g of the TiO₂ in 0.005 M HCl was used for the absorption of ⁶⁸Ge and 0.1 M HCl was used for the desorption of ⁶⁸Ga. Kozlova and colleague's work was used as a basis for this work. In this study five commercially available TiO₂ metal oxide materials, STMI TiO₂, Sigma-Aldrich rutile TiO₂, Sigma-Aldrich anatase TiO₂, Aeroxide® P-25 TiO₂ and Aerolyst® TiO₂ were evaluated for the absorption of ⁶⁸Ge and desorption of ⁶⁸Ga by varying TiO₂ particle size, heat treated or unheated and varying the HCl concentration (0.005 M - 0.1 M) for the loading of ⁶⁸Ge and stripping of ⁶⁸Ga.

Characteristics of the TiO₂ metal oxide such as morphology, particle size and composition were assessed and evaluated for their impact upon the ⁶⁸Ge loading obtained under acidic conditions. The higher loading of ⁶⁸Ge obtained corresponded well to small particle size as determined by XRD, SEM, TEM and BET techniques.

The STMI TiO₂ (>200 μm, unheated, 0.005 M HCl), Aeroxide® P-25 TiO₂ (heat-treated at 850 °C, 0.1 M and 0.005 M HCl) and Aerolyst® TiO₂ (90-212 μm, unheated, 0.1 M HCl), showed the best absorption qualities of ⁶⁸Ge at 100%. This source of TiO₂ was used to bench-mark further experiments as the manufacturing of the TiO₂ product came to an abrupt end. Both the Sigma Aldrich TiO₂ (rutile and anatase) showed no absorption of ⁶⁸Ge at any particle size or heating profile. The Evonik Aeroxide® TiO₂ (heated, 0.1 M and 0.005 M HCl) and Aerolyst® TiO₂ (90-212 μm, unheated, 0.1 M HCl), were pursued for further investigations.

Between the two sorbents (Aeroxide® P-25 and Aerolyst®), the Aerolyst® makes the better sorbent for a ⁶⁸Ga generator, as the ⁶⁸Ga desorption was marginally better than when Aeroxide® TiO₂ was used. Additionally, the study also found that no heat was required when the Aerolyst® was used as a sorbent. This is particularly important in sorbents as less time

and energy is required for modification. Nevertheless, the use of either of the sorbents produced a $^{68}\text{Ge}/^{68}\text{Ga}$ generator that had vastly fewer impurities than the existing production method in use in iThemba LABS, making this a $^{68}\text{Ge}/^{68}\text{Ga}$ generator that can be regarded as ultrapure.

A 15 mCi Aerolyst® TiO_2 based $^{68}\text{Ge}/^{68}\text{Ga}$ generator and Aeroxide® TiO_2 based $^{68}\text{Ge}/^{68}\text{Ga}$ generator system was evaluated over 12 months and it was shown that the ^{68}Ga elution of the Aerolyst® TiO_2 based $^{68}\text{Ge}/^{68}\text{Ga}$ generator was 54% at over 300 elutions and the ^{68}Ga elution of Aeroxide® TiO_2 was only 40% at over 300 elutions. For both sources of TiO_2 , the ^{68}Ga elutions appeared relatively stable throughout the 300 elutions, displaying good stability and low chemical degradation over the 12 month period. However, the ^{68}Ge breakthrough for the Aerolyst® TiO_2 metal oxide for the 300 elutions was averaging at about 0.05% compared to less than 0.05% for the Aeroxide® TiO_2 metal oxide. The Aerolyst® TiO_2 based $^{68}\text{Ge}/^{68}\text{Ga}$ generator was further investigated for metal impurities and it was shown that for a random metal analysis of the 300 daily elutions (eluate), the metal ion impurities of Zn, Fe, Sn, Ti, Cu, Al, Ga and Ge were found to be <1 ppm for each element.

The discovery of the relevancy of the Aerolyst® TiO_2 source was extremely valuable for the production of $^{68}\text{Ge}/^{68}\text{Ga}$ generators as it expedites the process by not requiring heat treatment, yet results in pure ^{68}Ga product. By using the SEM, TEM XRD and XRF techniques, the current study demonstrated that Aerolyst® TiO_2 metal oxide applied as a sorbent in the sorption of the ^{68}Ga radionuclide has the characteristics required to function in the $^{68}\text{Ge}/^{68}\text{Ga}$ generator capacity. It was possible to deduce the ^{68}Ga efficiency, ^{68}Ge breakthrough and metal analysis. This showed that a successful $^{68}\text{Ge}/^{68}\text{Ga}$ generator was achieved. Despite several other studies that have been conducted on $^{68}\text{Ge}/^{68}\text{Ga}$ generators, no other attempts have been made to provide information about the sorbent modifications. Through this study, it was shown that the Aerolyst® metal oxide can contribute considerably to the development of a TiO_2 based $^{68}\text{Ge}/^{68}\text{Ga}$ generator. This study, also described for the first time, a controlled investigation which compare and quantified the differences between the commercially available TiO_2 metal oxides. This study has three immediate benefits:

- (a) By characterization of the various TiO_2 sources by XRD and XRF, techniques, the identification of phase and particle size as well as level of purities were confirmed.

- (b) When SEM and TEM of the of Aeroxide® and Aerolyst® TiO₂ metal oxide were performed, information covering particle size, crystallinity and morphology was obtained.
- (c) Consequently, insight into the finer details about the behaviour of the TiO₂ sources during ⁶⁸Ge loading, ⁶⁸Ga elution, breakthrough analysis and metal impurity analysis were deduced.
- (d) Understanding of the factors affecting phase stability and phase transformation was important to design and controllably manipulate phase types and concentrations for more efficient use.

5.1 Recommendations and Future Work

To further develop understanding of a maximum ⁶⁸Ga efficiency accompanied by a non-existent ⁶⁸Ge breakthrough, future larger studies with statistical analyses of a TiO₂ based ⁶⁸Ge/⁶⁸Ga generator are of great interest. More research in this area is necessary before meaningful decision can be taken for the TiO₂ based ⁶⁸Ge/⁶⁸Ga generator. Secondly, despite its long clinical success, ⁶⁸Ge/⁶⁸Ga generators have a number of problems in use: leaking of columns which are attributed to degradation of the metal oxides and safety concerns. Several questions remain to be solved about the safety of the prolonged use of the ⁶⁸Ge/⁶⁸Ga generators. Therefore, it is recommended that a higher than 15 mCi generator be set up using the Aerolyst® TiO₂ metal oxide, eluted daily such that the ⁶⁸Ga eluted from the generator can be effectively, and directly, used for the labelling of peptides. Breakthrough studies, thereafter, should commence, and because this model is readily available, the values of the breakthrough of the Aerolyst® TiO₂ metal oxide will be closely assessed in an attempt to reduce them considerably. Results from such an exercise will be published in the near future. Further work on the Aerolyst® TiO₂ metal oxides should be focused on their treatment, as well as the assessment of their long-term stability.

Chapter Six

REFERENCES

- Aardaneh, K. and Van Der Walt, T.N. (2006). *Journal of Radioanalytical and Nuclear Chemistry*, vol. 268, no. 1, pp. 25-32.
- Antunes, P., Ginja, M., Zhang, H., Waser, B., Baum, R.P. and Reubi, J.C. (2007). Gallium-labelled DOTA-conjugated somatostatin analogues superior to those labelled with other radiometals? *European Journal of Nuclear Medicine and Molecular Imaging*, vol. 34, pp. 982–93.
- Bao, B. and Song, M. (1996). A new $^{68}\text{Ge}/^{68}\text{Ga}$ generator based on CeO_2 , *Journal of Radioanalytical Nuclear Chemistry*, vol. 213 no. 1, pp. 233–238.
- Barnes, G. and Gentle, I. (2005). *Interfacial science: An Introduction*, Oxford University Press Oxford, United Kingdom.
- Baum, R.P. and Roësch, F. (2012) *Theranostic, Ga-68 and other radionuclides: A Pathway to Personalized Diagnosis and Treatment. Radiotherapy and Molecular Imaging*, Springer Heildeberg, New York, pp. 594 – 600.
- Bauwens, M., Cheko, R. and Van Billoen, H. (2010). Optimal Buffer Choices for the Radiosynthesis of ^{68}Ga -DOTATOC for Clinical Application, *Nuclear Medicine Communication*, vol. 31, pp. 753-758.
- Bjørnstad, T. (2004). “Industrial radionuclide generators — status and perspectives”, paper presented at Conf. on Tracer and Tracing Methods, Ciechocinek, Poland.
- Brady, G.S. (1971). *Materials Handbook*. New York: McGraw-Hill.
- Breeman, W.A.P and Verbruggen, A.M. (2007). The $^{68}\text{Ge}/^{68}\text{Ga}$ generator has high potential, but when can we use ^{68}Ga -labelled tracers in clinical routine? *European Journal of Nuclear Medicine and Molecular Imaging*, vol. 34, pp. 978–981.

- Breeman, W.A.P., de Jong, M., de Blois, E., Bernard, B.F., Konijnenberg, M. and Krenning, E.P. (2005). Radiolabelling DOTA-peptides with ^{68}Ga , *European Journal of Nuclear Medicine*, vol. 32, pp. 478–485.
- Breeman, W.A.P., Marion, J., Visser, T.J., Erion, J.L., Krenning, E.P. (2003). Optimising conditions for radiolabelling of DOTA-peptides with ^{90}Y , ^{111}In and ^{177}Lu at high specific activities, *European Journal of Nuclear Medicine for Molecular Imaging*, vol. 33, pp. 917 – 920.
- Burger, C. and Townsend, D.W. (2003). Basic of PET Scanning. In: Schultess, G. *Clinical PET, PET/CT and SPECT/CT*. Lippincott, vol. 3, pp. 14 – 39.
- Caletka, R. and Kotas, P. (2004). Separation of Germanium from some elements by adsorption of silica gel. *Journal of Radioanalytical Chemistry*, vol. 21, pp. 349-353.
- Carter, H. K. Hamilton, J. H. Ramayya, A. V. and Pinajian J. J. (1968). Evidence of a O^+ State in ^{65}Zn populated by “Ga”. *Physics Revision*, vol. 174, pg. 1329.
- Cesareo, R., Gigante, G.E., Castellano, A. and Iwanczyk, J.S. (2000). Portable Systems for Energy-dispersive X-ray Fluorescence, in: *Encyclopedia of Analytical Chemistry*, R. A. Meyers (Ed.), J. Wiley & Sons Ltd., Chichester, pp. 13327-13338.
- Chakravarty, R., Shukla, R., Ram, R., Tyagi, A.K., Dash, A. and Venkatesh M. (2011). Development of a nano-zirconia based $^{68}\text{Ge}/^{68}\text{Ga}$ generator for biomedical applications, *Nuclear of Medical Biology*, vol. 38, no. 4, pp. 575-83.
- Clarke, A. R. (2002). *Microscopy Techniques for Materials Science*. CRC Press (electronic resource)
- De Blois, E, Sze-Chan, H., Naidoo, C, Prince, D., Krenning, E.P. and Breeman, W.A. (2011). Characteristics of SnO_2 -based $^{68}\text{Ge}/^{68}\text{Ga}$ generator and aspects of radiolabelling DOTA-peptides. *Applied Radiation Isotope*, vol. 69, pp. 308–315.
- Decristoforo, C., Knopp, R., von Guggenberg, E., Rupprich, M., Dreger, T., and Hess, A. (2007). A fully automated synthesis for the preparation of ^{68}Ga -labelled peptides. *Nuclear Medicine Communication*, vol. 28, pp. 870–875.
- Decristoforo, C., Von Guggenberg, E., Haubner, R., Rupprich, M., Schwarz, S. and Virgolini, I. (2005). Radiolabelling of DOTA-derivatised peptides with ^{68}Ga via a direct approach: optimization and routine clinical application, 27th

- International Symposium: Radioactive isotopes in clinical medicine and research, Nuclear Medicine, vol. 6, pg. 191.
- Depero, L.E., Bonzi, P., Zocchi, M., Casale, M. and De Michele, G. (1993). "Study of the Anatase-Rutile Transformation in TiO₂ Powders Obtained by Laser-Induced Synthesis," Journal of Materials Research, vol. 8, no. 10, pp. 2709-2715.
- Deutsch, E. (1993). Clinical PET: its time has come? Journal of Nuclear Medicine, vol. 34, pp. 1132–1133.
- Egerton, R. F. (2005). Physical principles of electron microscopy: an introduction to TEM, SEM, and AEM. Springer, New York, pg. 202.
- Erhardt, G.J. and Welsh, M.K. (1978). A new germanium ⁶⁸Ge/⁶⁸Ga generator. Journal of Nuclear Medicine, vol. 19, pp. 925-929.
- Gleason, G.I. (1960). A positron cow. International Journal of Applied Radiation and Isotopes, vol. 8, pp. 90–94.
- Goldstein, J. (2003). Scanning Electron Microscopy and X-ray Microanalysis. Kluwer Academic/Plenum Publishers, pg. 689.
- Greene, W.T. and Tucker, W.D. (1961). An Improved gallium-68 cow, Internal Journal of Applied Radiation and Isotopes, vol. 12, pg. 62.
- Hechel, J. and Ryon, R.W. (2001). Polarized Beam X-ray Fluorescence Analysis, Chapter 10 in: Handbook of X-ray Spectrometry, 2nd edition, (R.E. Van Grieken and A.A. Markowicz, Eds.), Marcel Dekker, New York.
- Henze, M. Schuhmacher, J. Hipp, P. Kowalski, J. Becker, D.W. and Doll, J. (2001). PET imaging of somatostatin receptors using [⁶⁸Ga] DOTA-D-Phe1-Tyr3-octreotide: first results in patients with meningiomas, Journal of Nuclear Medicine, vol. 4, pp. 1053–1056.
- Hofmann, M., Mäecke, H., Borner, R., Weckesser, E., Schoffski, P. and Oei, L. (2001). Bio-kinetics and imaging with the somatostatin receptor PET radio-ligand ⁶⁸Ga-DOTATOC, European Journal of Nuclear Medicine, vol. 28, pp. 1751–1757.
- Horiguchi, H., Kumahora, H., Inoue, H. and Voshizawa, Y. (1983). "Excitation functions of Ge(p,xnyp) reactions and production of ⁶⁸Ge", International Journal of Applied Radiation and Isotopes, vol. 34, pg. 1531.

- International Atomic Energy Agency, (2005). Report of Consultants Meeting on Radionuclide Generators for Industrial Radiotracer Technology, IAEA, Vienna, Austria.
- International Atomic Energy Agency, (2013). Radiotracer Generators for Industrial Applications, IAEA Radiation Technology Series Publications, Vienna, Austria.
- Keidar, Z., Israel, O and Krausz, Y. (2003). SPECT/CT in tumour imaging: technical aspects and clinical applications, *Journal of Nuclear Medicine*, vol. 33, pp. 205-208.
- Kopecky, P. and Mudrova, B. (1974) $^{68}\text{Ge}/^{68}\text{Ga}$ generator for the production of ^{68}Ga in ionic form, *International Journal of Applied Radiation and Isotopes*, vol. 25, pp. 263-268.
- Kopecky, P., Mudrova', B. and Svoboda, K. (1973). The study of conditions for the preparation and utilization of $^{68}\text{Ge}/^{68}\text{Ga}$ generator, *International Journal of Applied Radiation and Isotopes*, vol. 24, pp. 73–80.
- Kozlova, M.D., Malinin, A.B., Kodina, G.E. and Sevastyanova, A.S. (1970). Radiopharmaceutical Department, Institute of Biophysics, Ministry of Public Health, Moscow, Russia, vol. 12, pg. 505.
- Lange, J. Hamilton, J. H. Little, P. E. HalTox, D. L. Morton, D. C. Whitlock, L. C. and Pinajian, J. J. (1973). E2-M1 admixture of transitions in “Zn”, *Physics Revision*, vol. 7, pg. 177.
- Lippens, B., and De Boer, J. (1965). Studies on pore systems in catalysts: V. the t method. *Journal of Catalysis*, vol. 4, pp. 319–323.
- Loc'h, C., Maziere, B. and Comar, D.A. (1980). New generator for ionic gallium-68, *Journal of Nuclear Medicine*, vol. 21, pp. 171–173.
- Mäecke, H.R., Hofmann, M. and Haberkorn, U. (2005). ^{68}Ga -labeled peptides in tumor imaging. *Journal of Nuclear Medicine*, vol. 46, no. 1, pp. 172S–178S.
- Makinen, T.J. Lankinen, P. Poyhonen, T. (2005) Comparisons of ^{18}F -FDG and ^{68}Ga PET imaging in the assessment of experimental osteomyelitis due to *Staphylococcus aureus*, *European Journal of Nuclear Molecular Imaging*, vol. 32, pp. 1259-1268.
- Mardsen, P.K. (2003). Detector technology challenges for nuclear medicine and PET, *Nuclear Instruments and Methods of Physical Research*; vol. 513, pp. 1 – 7.

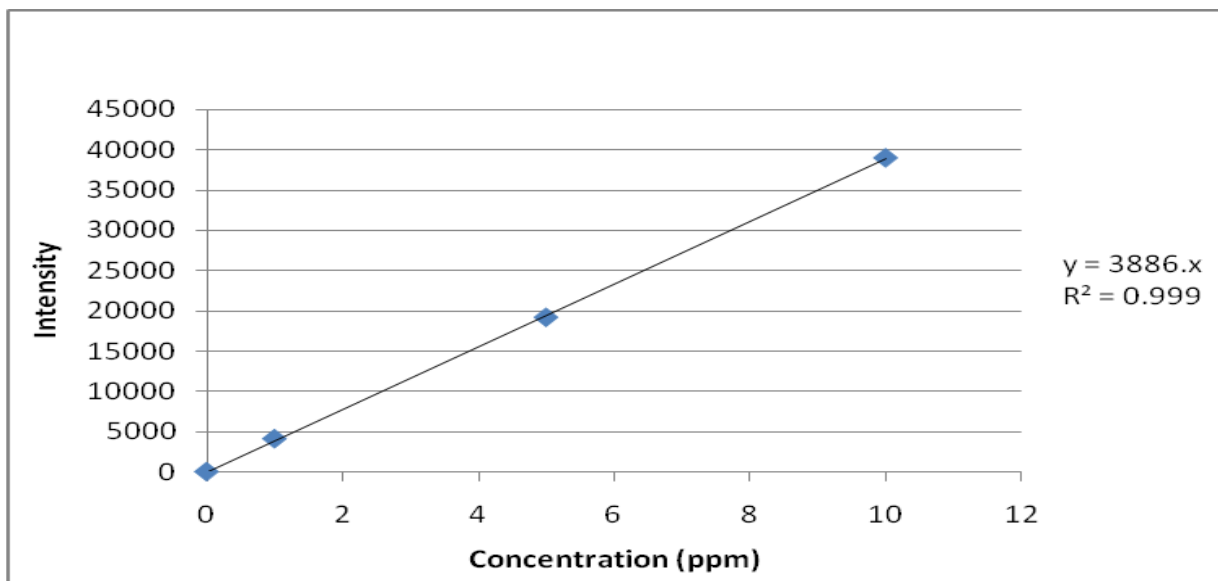


Figure 7.8: Calibration curve of Gallium metal element

